FINAL PUBLISHABLE JRP REPORT

JRP-Contract number	ENG08
JRP short name	METROFISSION
JRP full title	Metrology for New Generation Nuclear Power Plants
Version numbers of latest contracted Annex Ia and Annex Ib against which the assessment will be made	Annex Ia: V1.2 Annex Ib: V1.0
Period covered (dates)	From 01 September 2010 to 31 August 2013
JRP-Coordinator	Lena Johansson
Name, title, organisation	National Physical Laboratory
Tel:	+44 (0)20 8943 8587
Email:	lena.johansson@npl.co.uk
JRP website address	http://projects.npl.co.uk/metrofission/
Other JRP-Partners	

NPL, United Kingdom
CEA, France
CEM, Spain
CIEMAT, Spain
CMI, Czech Republic
CNAM, France
ENEA, Italy
IFIN-HH, Romania
JRC, EC
LNE, France
PTB, Germany
SMU, Slovakia

REG-Researcher
(associated Home Organisation)

Mr Michele Scervini
UCAM, United Kingdom

Start date:1st Jan 2011
Duration: 30 months

Report Status: PU Public

EMRP
European Metrology Research Programme
Programme of EURAMET
The EMRP is jointly funded by the EMRP participating countries within EURAMET and the European Union

TABLE OF CONTENTS

1 Executive Summary

Introduction

Society demands energy supplies that are secure, sustainable and of high quality. In the next decade, Europe is facing potential energy shortages as oil and gas supplies run down and nuclear power facilities age. Pressure to reduce the greenhouse gas emissions has led to a requirement for the development of a new generation of nuclear power plants in Europe. This project developed the necessary metrology infrastructure to enable measurement of key parameters associated with new generation nuclear power plants in order to ensure that energy suppliers and regulators develop a safe and secure nuclear energy supply.

There are several designs (typically six) for the proposed Generation IV nuclear reactors. The main differences between current nuclear reactors and Generation IV nuclear reactors are the type of fuel, the higher energy of neutrons required and a closed fuel cycle design that enables the fuel to be recycled leading to more efficient use of natural resources, minimisation of waste and maintained proliferation resistance. Generation IV reactors also operate at high temperatures and are capable of utilising industrial process heat to improve their efficiency and economy. In these reactors the temperatures will be much higher (i.e. above 1000 °C) than conventional reactors (i.e. 500 °C).

Therefore, generation IV reactors pose the following metrological problems, which this project aimed to answer: How can the temperatures be accurately measured, as existing thermocouple-based methods cannot be used at these temperatures and in this environment? What materials could be used in these reactors and how do we determine the thermal properties of these potential reactor materials? What nuclear data and radiation measurement techniques are needed to support the safe and effective operation of Generation IV reactors?

Technical results from the project:

Improved temperature measurement for nuclear power plant applications

New temperature sensors and methods for *in-situ* measurements in nuclear power plants have been investigated and developed with an emphasis on extending the measurement range to higher temperatures and characterising, limiting, or completely eliminating the sensor drift in a high-temperature, high-neutron-flux environments. A new reference temperature fixed point at 1153.8 ^{o}C (above the existing copper point) was developed and is available for post-irradiation studies of thermocouples or as a calibration service. A thermocouple from the Mo/Nb family was identified as potentially suitable for the nuclear environment. It was constructed by the company Thermocoax and tested by project partners in terms of its reference functions, stability, and thermoelectric homogeneity. However the studies showed rather disappointing stability results and will require further investigation in the future. Self-validation methods for thermocouples as a means to reduce or eliminate in-situ drift related problems have been developed that are suitable for use in the nuclear industry. In addition, practical primary acoustic thermometry, an inherently drift-less technique, has been tested through the construction of a demonstrator. This so far successful method could be used to assess the drift performance of more conventional sensors or as an in-situ temperature sensing method in its own right.

Thermal properties of advanced materials for nuclear design

Thermodynamic models have been developed and parameterised for a range of major and minor actinide containing systems relevant to nuclear fuels (both in reactors and during reprocessing) and coolants. These models have allowed the project to make predictions related to high-temperature phase equilibria (e.g. phase transformation temperatures) of these materials, which was validated partly by comparison with experimental observations (outside of this project). Data was critically assessed to represent the potential interaction between the sodium coolant and the MOX nuclear fuel, taken to be based on $(U,Pu)O_{2,}$ and incorporating minor actinides such as neptunium and americium. Data for the fission products and containment materials have also been reviewed and new data assessed to represent the interaction between them, the sodium coolant and the environment, in order to permit the calculation of phase and chemical equilibria for severe

accident scenarios. These validated models will support the selection of the most appropriate materials for fuel and coolants of Generation IV Reactors.

Reference facilities for the measurement of thermophysical properties (thermal diffusivity, normal spectral emissivity, thermal expansion and specific heat) of solid materials up to 1500 °C or 2000 °C (depending on which thermal property) have been developed. They have been applied to the thermal characterisation of materials at high temperatures and enabled an improvement in the traceability of the thermal properties measurements performed at high temperature by nuclear research laboratories. Suitable candidate materials to serve as "transfer reference materials" for high temperature thermal properties measurements have been identified and characterised. The thermophysical properties of high purity 4N tungsten produced by *Plansee*, isostatic graphite grade R6650P5 from SGL Carbon group, magnesium oxide (powder) and nickel and zirconium dioxide (homogeneous solid materials) were selected because they are non-radioactive, stable at the temperatures of interest, and because of their relevance to thermal property measurements on nuclear materials. The next stage of validation of ISO graphite as a suitable reference material is scheduled for June 2015. Two of the project partners have been invited to participate in an APMP T-S.9 TCT thermal diffusivity supplementary comparison led by NMIJ (Japan), which will include NMI participants from NPL, LNE, KRISS (Korea), NIM (China), CMS/ITRI (Taiwan).

Improved metrology for neutron cross section measurements

An easy-to-use calibrated neutron fluence standard was developed and its potential for the determination of cross sections of interest was demonstrated by a number of neutron induced fission cross section measurements on ^{240}Pu and ^{242}Pu with mono-energetic neutron beams produced at two different NMIs, i.e. at the Van de Graaff accelerator and the cyclotron of PTB and at the Van de Graaff accelerator of NPL. The measurements were performed using gas filled detectors, consisting of a Frisch-gridded ionisation chamber containing the plutonium sample, mounted back to back to a parallel plate chamber containing a ^{238}U sample. The neutron fluence was successfully measured in parallel with the ^{238}U parallel plate chamber and with the fixed neutron fluence monitors available at the respective institutes. The availability of this transfer instrument for neutron fluence measurements will improve future nuclear data in the form of reduced measurement uncertainties[1].

Development of nuclear data

Alpha-particle emission probabilities of ^{238}U with certified isotopic composition have been determined and spectrometric measurements completed. The accuracy of the alpha particle emission probabilities of ^{238}U was improved by one order of magnitude compared to previously recommended values. Furthermore, a unique, state-of-the-art cryogenic detector was used as a means to determine the shape of beta spectra of ^{63}Ni (a pure beta transmitter). This is innovative approach that offers exceptional characteristics in terms of energy resolution and detection efficiency over a wide energy range. The experimental determination of beta spectrum shapes is essential for verifying and/or modifying existing theoretical models. The measurements of the beta-spectrum of ^{63}Ni have been made available in scientific literature and will be part of future international evaluation of nuclear data.

Improved measurement techniques for radionuclides

The measurement techniques that have been developed were aimed at providing an ability to perform on-site radioactivity measurements, by the development of a portable Triple to Double Coincidence Ratio (TDCR) system. Four prototypes of the portable TDCR system have been completed and validated against the international reference system for a range of beta-emitters. An improved digital acquisition system was developed for the portable TDCR. The digital electronics were also tested on other detector systems in order to assess whether they can allow for pulse-shape discrimination (which can be used for discrimination between different types of radiation) and measurement at higher count-rates (which would be applicable to the nuclear industry). The digital systems developed are state of the art systems with hardware that can acquire data at sampling rates of 10^9 s^{-1} and can be implemented on two channels (coincidence counting) or three channels (TDCR) detector systems. The overall system has been made available for applications on-site in nuclear power plants.

[1] See"Uncertainty and target accuracy assessment for innovative systems using recent covariance data evaluations" published by a working party of the OECD Nuclear Energy Agency in 2008.

2 Project context, rationale and objectives

2.1 New generation nuclear power plants

Society demands energy supplies that are secure, sustainable and of high quality. In the next decade, Europe is facing potential energy shortages as oil and gas supplies run down and nuclear power facilities age. Pressure to reduce the greenhouse gas emissions has led to a requirement for the development of a new generation of nuclear power plants in Europe.

This project developed the necessary infrastructure to enable measurement of the key parameters associated with new generation nuclear power plants, in the area of materials, temperature, neutron fluence, nuclear data and radioactivity to ensure that energy suppliers and regulators can work towards an energy secure future within a metrology framework.

There are several designs (typically six) for the proposed Generation IV nuclear reactors. The main differences between current nuclear reactors and Generation IV nuclear reactors are the type of fuel, the higher energy of neutrons required to fission and the fact that the fuel cycle is closed enabling the fuel to be recycled enabling a more efficient use of natural resources, minimisation of waste and maintained proliferation resistance. Generation IV reactors also operate at high temperatures and are capable of utilising industrial process heat to improve their efficiency and economy. In these reactors the temperatures will be much higher (i.e. above 1000 °C) than conventional reactors (i.e. 500 °C).

Therefore, generation IV reactors pose the following metrological problems, which this project aimed to answer: How can the temperatures be accurately measured, as existing thermocouple-based methods cannot be used at these temperatures and in this environment? What materials should be used in these reactors and what are their thermal properties? What nuclear data and radiation measurement techniques are needed to support the safe and effective operation of Generation IV reactors?

2.2 Scientific and Technical Objectives

Therefore the key aims of the project were to:

- **Develop improved temperature measurement for nuclear power plant applications** by providing metrology for measurements at the higher temperatures required for operating the next generation of nuclear power plants.
- **Characterise thermal properties of advanced materials for nuclear design** in order to assist with construction of the new generation of nuclear power plants. Understanding the behaviour of nuclear fuels, coolant and materials used for the reactor enclosure is vital to the design and safe operation of nuclear reactors. This includes developing models of the thermodynamic behaviour and the ability to measure and characterise thermal physical properties of relevant materials (specific heat capacity, thermal diffusivity, thermal expansion, and emissivity). In some cases, these properties can already be measured at high temperatures; however these measurements often lack traceability to the SI above 800 °C. Therefore, reference metrological methods need to be implemented or improved for measurements up to 2000 °C (1500 °C in the case of specific heat of solids).
- **Develop improved metrology for determination of high-energy neutron cross sections**. New fast reactor designs will involve materials exposed to higher energy neutron fields. The current nuclear databases concentrate on thermal energies, so much work is needed on nuclear data at higher energies. Advantage will be taken of NMI experience in neutron metrology, particularly fluence measurements, to improve cross section measurements of interest to new generation power plants and fuel cycles. In this respect, an important objective of the project was to establish an easy-to-use secondary fluence standard and to demonstrate its potential for the determination of cross sections of actual interest and the improvement of nuclear data standards in the form of reduced measurement uncertainties. The last point is particularly in line with the "*Uncertainty and target accuracy assessment for innovative systems using recent covariance data evaluation*s" published by a working party of the OECD Nuclear Energy Agency in 2008.

- **Produce nuclear data for the fuel cycle of new nuclear power plants and to provide important data regarding the thermal energy released in the reactor core from minor actinides present in the fuel.** The heavier actinides and their decay products have generated increased interest in recent years because of their role in the foreseen development and adoption of nuclear power plants in whose fuels they will be present in controlled amounts. Uranium-238 (^{238}U) is the dominant fissile material in the fuel of new reactors and is a nuclide that has been highlighted in a recent review by the IAEA[2] as an actinide that requires new and improved nuclear data. Furthermore, the decay heat produced by fission products, amounting to 8 % of the energy generated during the fission process, needs to be well characterised for safe operations (reactor shutdown, post irradiation handling of nuclear fuels). This decay heat corresponds to the radiant energy (beta, gamma) emitted by the natural decay of these nuclides, which is imparted to surrounding medium. Therefore the second part of this objective was to improve knowledge of beta spectra.
- **Develop improved measurement techniques for radioactivity for safe and efficient operation of new nuclear power plants.** The TDCR (Triple-to-Double-Coincidence-Ratio) method is the only available detection method for beta particles (emitted from e.g. ^{3}H and ^{241}Pu) that can deliver a result without preceding calibration. It also has the potential to reduce uncertainties by a factor of two. By miniaturising this instrument it can be used in nuclear power plants, bringing benefits to activity measurements *in-situ*.

3 Scientific and technological results and foreground

3.1 New high temperature references tailored to assess performance of current and new thermocouples

Conventional thermocouples used in the nuclear industry (Type K and N, for instance) start drifting significantly above the range 1000 °C to 1100 °C depending on their wire dimensions. Above these temperatures the most stable thermocouple types (Type R, S, B…) endure important transmutations under ionising radiation. Therefore thermocouple manufacturers are seeking possible alternative types to be capable of long-term stable operation at the highest temperatures with reduced risk of transmutation.

Operating for a prolonged period in an intense radiation environment places demands on all measuring apparatus, but the demands on temperature-measuring equipment are among the most extreme.

The reason is that the temperature-dependent properties of a thermometer typically depend on fine details of the electronic and mechanical structure of the thermometric material. When placed into a high-radiation environment these details are easily affected and the thermometer immediately begins to drift from its calibrated state. Thus it is desirable to choose a thermometry technique which has the possibility of *in situ* calibration; has a thermometric material which is insensitive to radiation; and is based on well-understood physics and engineering principles.

In this project, temperature sensors were developed and reference fixed point cells developed and adapted to in-situ usage. The expectations in this field are mostly oriented towards a better reliability of the instrumentation working in harsh environments with high neutron fluxes in conjunction with high temperatures.

3.1.1 Practical temperature references

There were two main motivations for the research on new temperature references. The first was to develop a new fixed point with materials, in principle, not prone to transmutation that can be used by the nuclear industry. The second was to develop self-validation techniques for thermocouples, which implied constructing and characterising miniature fixed point cells to be attached to thermocouples in order to ensure their in-situ recalibration. For both activities, the outcome of the project was successful and offers a large area of applications in the future, beyond the nuclear industry needs.

3.1.1.1 Fe-C fixed point

To achieve the realisation of a temperature reference point suitable for post-irradiation drift studies for thermocouples, the choice of the material stood on two requirements: a melting temperature close to 1200

[2] A.L. Nichols, IAEA, Actinide Decay Data: Measurement requirements identified to date (IAEA – October 2008)

°C and materials with low neutron capture cross-section. The Fe-C eutectic point (~1154 °C) was the best candidate. This fixed point was studied about ten years ago at the National Metrology Institute of Japan [8] and at LNE and CNAM [9] but mainly for the purposes of non-contact thermometry. It was considered as the best choice for this project given the low neutron capture cross-section of iron.

Conventional types of fixed-point cells (with typically 100-mm immersion depth, when adapted to Pt/Pd thermocouples) were constructed and characterised at NPL, LNE and CNAM. The cells were also compared to assess the equivalence of the phase transition. A total of five cells were compared at NPL using two Pt/Pd thermocouples, supplied by the LNE and CNAM [3-5]. Different parameters were varied in order to derive their influence on the measured melting temperatures. For instance, the effects of the amount of carbon in the Fe-C mixture during the filling of the cells, the graphite used for the construction of the crucibles, the origin of the high-purity iron and the construction site and method were analysed [3]. This allowed estimation of the reproducibility of these new fixed-point cells, as well as observing the differences in terms of melting temperatures. Figure 1 indicates that the level of agreement between measurements with two Pt/Pd thermocouples on a single cell was better than 0.2 °C whereas the agreement between four different cells as determined with a single thermocouple was well within 0.1 °C.

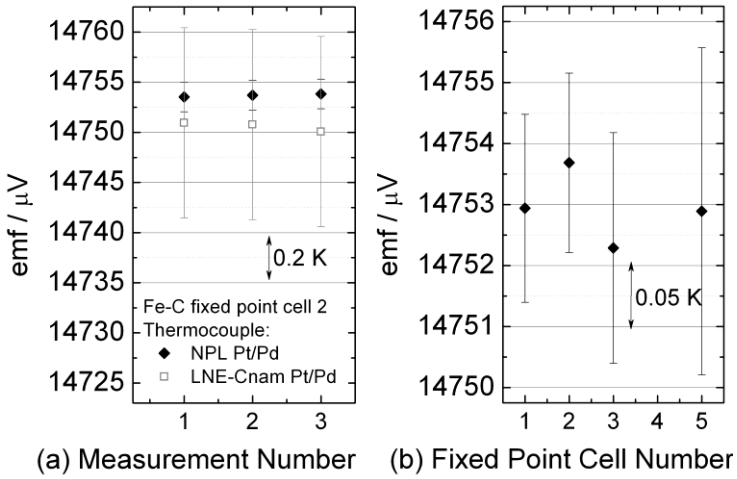

Figure 1. (a) Temperature measurements of Fe-C fixed-point cell #2 observed using the NPL (diamonds) and LNE and CNAM (open squares) Pt/Pd thermocouples. (b) Agreement of the fixed-point temperature, using the NPL thermocouple, with cells 1, 2, 3 and 5 – here each point represents the mean of three consecutive melting temperatures. Error bars indicate the expanded uncertainty for the thermocouple in each cell [3].

Figure 2 shows the effect of varying four parameters on the melting temperatures as measured with the two Pt/Pd thermocouples. All the studied parameters gave influences below 0.15 °C. It is very likely that these levels of agreement and uncertainties are mostly due to the stability of the thermocouples used in this study. Moreover, the robustness of the cells is considered as very satisfactory after performing tens of melt/freeze cycles.

To complete the characterisation of this new fixed point, traceable temperature measurements were performed in order to assign a temperature to the melting transition. The temperature assignment was performed both at NPL, LNE and CNAM on their respective cells. The temperatures obtained at LNE and CNAM on two different cells were 1153.84 °C and 1153.79 °C with an uncertainty of ± 0.35 °C (*k=2*). The measurements performed at NPL by radiation thermometry gave a very close melting temperature: 1153.58 ± 0.34 °C (*k=2*). The final step of the work on Fe-C fixed point was the miniaturisation of the cells for their application as *in-situ* self-validation devices.

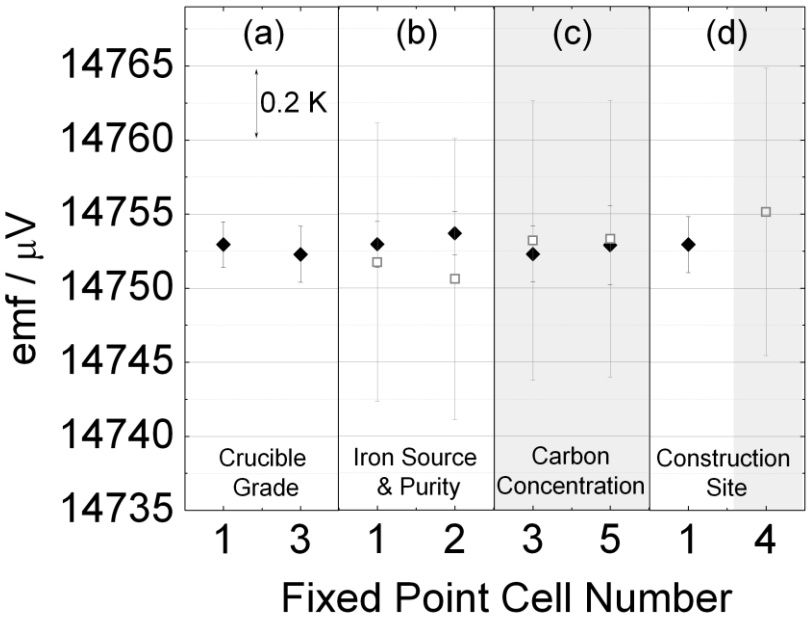

Figure 2. Melting point agreement after changing only (a) the grade of graphite used to manufacture the crucible, (b) the source (and the purity) of iron, (c) the initial concentration of graphite or (d) the construction site. Points represent the mean of three consecutive melting temperatures, measured with NPL Pt/Pd thermocouple (diamonds) or LNE and CNAM thermocouple (open squares), at NPL site except LNE and CNAM thermocouple measurements of cells 3, 4 and 5 (measured at LNE and CNAM site). Error bars indicate the expanded uncertainty for each thermocouple in each cell [3].

3.1.1.2 Self-validation techniques

Thermocouples may drift significantly in use, both due to the thermal environment and in a nuclear environment, due to continuous neutron irradiation. The objective was to demonstrate the practicality of self-validation methods for thermocouples and their usefulness as a means for the in-situ recalibration of temperature sensors. Besides constructing reliable, robust and repeatable devices it is also important to solve the difficulties of an uncontrolled thermal environment.

The first step of this work was the design of self-validation artefacts i.e. thermocouples with a miniaturised fixed-point cell attached (see Figure 3), which were adapted to currently used thermocouples. NPL, LNE and CNAM have tried different designs of cells in continuation of the developments achieved to date in both institutes on self-validation techniques.

At NPL two different designs were tested successfully at the Co-C (1324 °C) temperature. These designs can accommodate integrated thermocouples [10] or sheathed thermocouples [11] (Figure 3).

The device developed by LNE and CNAM and tested at the gold, copper and iron-carbon fixed points is shown in Figure 4. This design was chosen in order to improve the robustness of the cells and to facilitate the filling process. However, the thermometer well is not surrounded by the metal as in normal fixed-point cells or as in the NPL “immersion-type” design (Figure 3(a)) and the mass of metal is only 2-3 g. This means that the thermocouple can sense the temperature of the furnace as much as the temperature of the metal. Therefore the measured melting and freezing temperatures are different and vary with varying furnace temperatures.

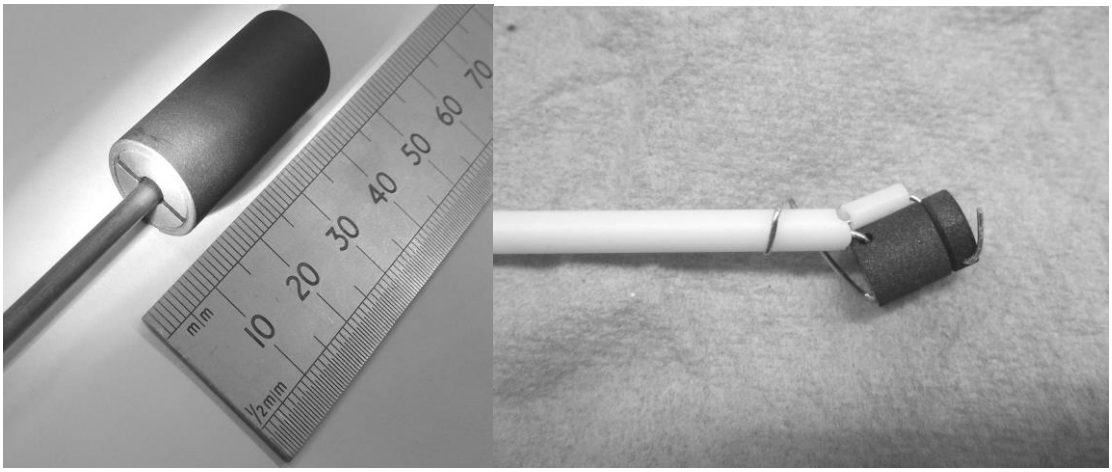

(a) (b)

Figure 3. Self-validation cells developed at NPL: (a) immersion-type cell [11] (b) integrated-type cell [10].

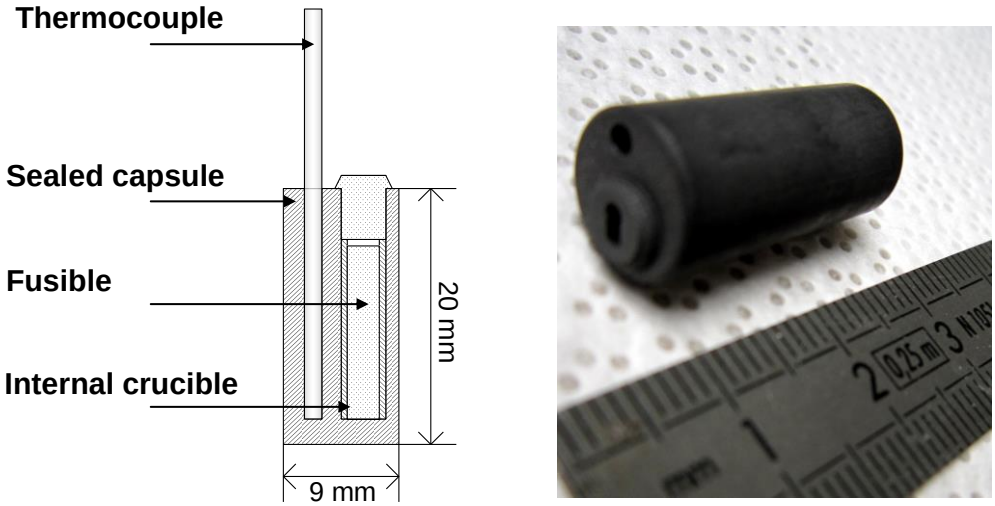

Figure 4. Schematic and photo of the microcells developed at LNE and CNAM

A typical melt and freeze plateau obtained with a copper microcell of the LNE and CNAM design can be seen in Figure 5. The difference observed between the melt and the freeze can reach several degrees and depends on the furnace offsets. Nevertheless, by tuning the furnace set-points, the difference between melt and freeze can be reduced and by an iterative process the thermocouple can be recalibrated *in-situ* with progressively lower uncertainties.

These techniques were applied to the Fe-C point both at NPL, LNE and CNAM. The repeatability of the melting temperatures observed at NPL with the “immersion-type” design, where about 9 g of eutectic ingot is contained in the cell, was very satisfactory and lie within a few tenths of a kelvin as can be seen in Figure 6.

In all cases the observed reproducibility with changing furnace conditions lies at most within a few degrees, with each of the different designs and fixed-point cells under study. These performances are in accordance with the needs commonly expressed in industry where a typical accuracy of ± 5 °C would be satisfactory.

The LNE and CNAM cells have however shown much larger melting ranges, as can be seen in Figure 7, because filling with powders leads to very small sizes of ingots and increased the effect of the thermal environment on the measured transition temperature. The next version of cells, presently under construction, will improve thermal anchoring of the thermocouple in the metal ingot and increase the mass of the ingot.

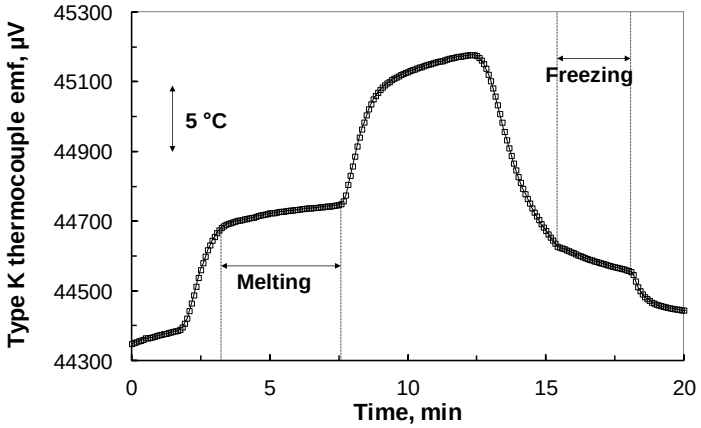

Figure 5. Melt and freeze cycle obtained with a Type K thermocouple within an LNE and CNAM copper microcell.

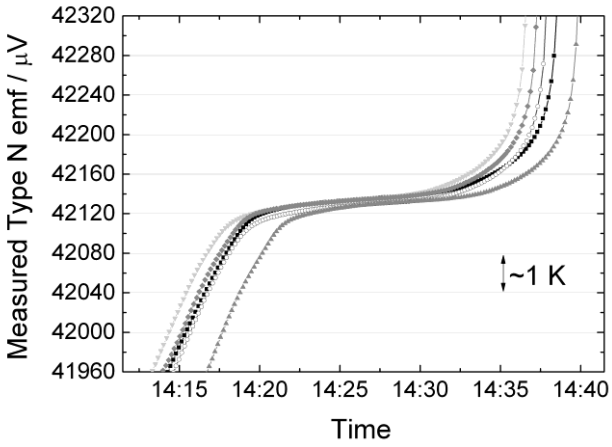

Figure 6. Melting plateaux measured with a mineral insulated metal sheathed Type N thermocouple on a Fe-C self-validating cell at NPL.

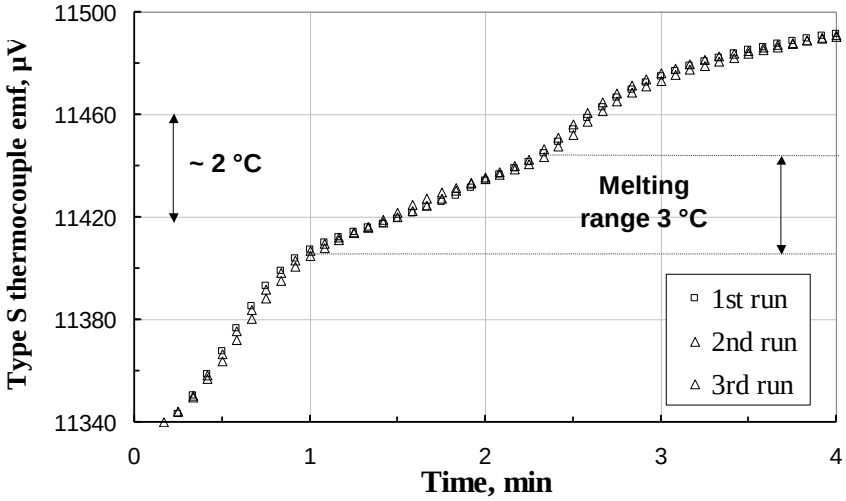

Figure 7. Melting plateaux measured with a mineral insulated metal sheathed type S thermocouple on a Fe-C self-validation cell at LNE and CNAM.

Long and repeated thermal exposures have been applied to the self-validating devices (cells and thermocouples) in order to assess their ability to correct for possible drift of the thermocouple and to ensure long-term performance.

Figure 8 shows a typical endurance test performed on a Type N thermocouple in an NPL “immersion-type” Fe-C cell. The cell was repeatedly heated to just above the Fe-C melting temperature and held at that temperature for a dwell period of 1 or 10 hours (the exposure time). The electromotive force (emf) of the thermocouple was recorded at each melting plateau occurrence and these are shown in Figure 8. As the fixed point cell is known (from non-contact thermometry measurements) to not have measurably drifted over this period, the major part of the observed drift is attributed to the drift of the thermocouple which therefore can be corrected easily.

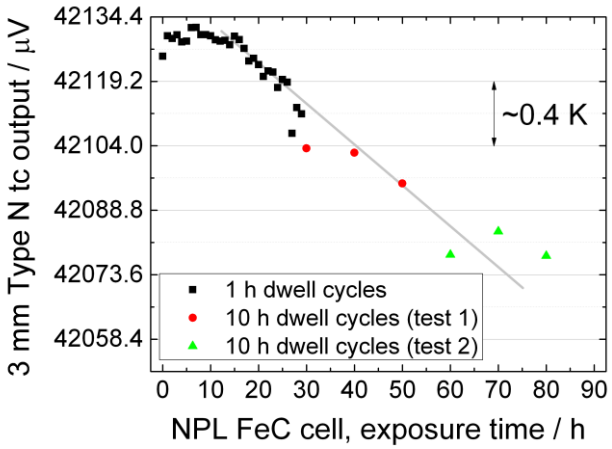

Figure 8. Measured fixed point transitions of the NPL self-validating Fe-C (svtc) cell showing the decay in thermocouple output with exposure time.

The overall performance of the self-validation devices was proven to be well within expectations and supports the usage of such techniques in various fields of industry and in particular, as far as Fe-C is concerned, in a nuclear environment at a temperature as high as 1154 °C.

3.1.2 Temperature Sensors

These sensors are supposed to be unaffected by transmutations or more adapted to harsh environment and should exhibit lower drifts. They also aim to address the need for improved measurements *in-situ* in terms of accuracy and reliability. The development of specific contact sensors based on materials having very low neutron capture cross-section (molybdenum and niobium), or contact sensors based on a different measurement technique (acoustic thermometer) are among the possible solutions.

3.1.2.1 Mo/Nb type thermocouples

The Mo/Nb thermocouple family offers, in principle, the rare features of long-term stable operation at the highest temperatures with reduced risk of transmutation. [12, 13]. Thermocoax (France), one of the world leading manufacturers of thermocouples, has recently collaborated with CEA to develop and characterise specific Mo/Nb thermocouples with dopants aimed at the stabilisation of the Seebeck coefficient of the wires [14]. This research led to a promising version of Mo/Nb thermocouples which was studied in this project.

The experimental work performed in this project on these thermocouples started with the study of their homogeneity in an oil bath at 200 °C. The results obtained (Figure 9) at this temperature were considered as satisfactory.

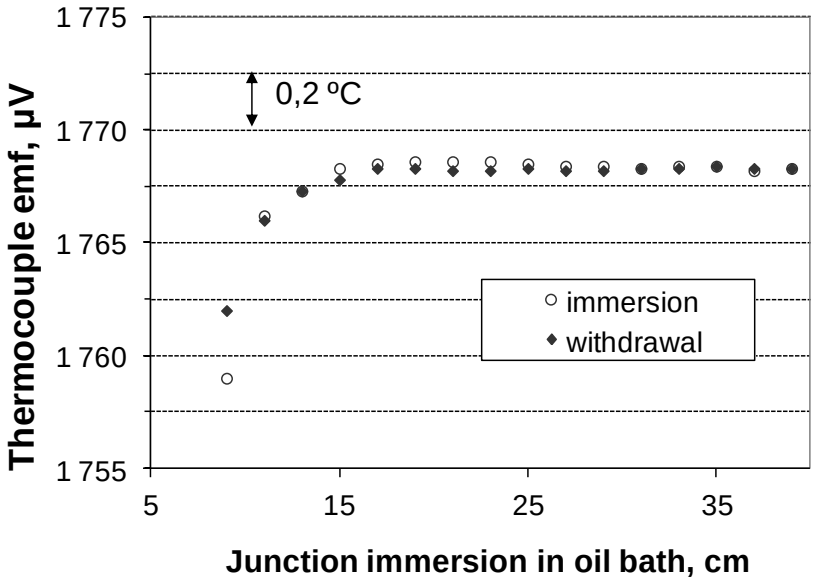

Figure 9. Immersion test performed at CEM on an alumina sheathed doped Mo/Nb thermocouple in an oil bath at 200 °C.

The subsequent tests at the silver fixed point have shown however that the thermocouples were not stable at high temperature and needed a thermal annealing. The temperature level for this heat treatment was advised by the manufacturer to be 1100 °C. A thermal annealing was therefore performed at CEM, LNE and CNAM during hundreds of hours at 1100 °C. So far, it did not prove sufficient to stabilise the thermocouples to the foreseen level of a few kelvins.

Figure 10 shows the evolution of the emf of a Mo-sheathed doped Mo/Nb thermocouple annealed during a period exceeding 200 hours.

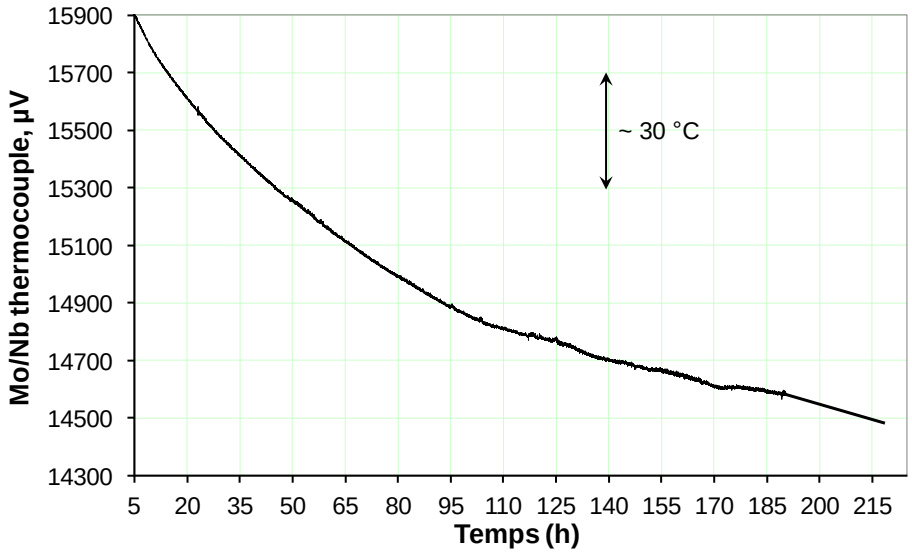

Figure 10. Monitoring of the emf of a Mo-sheathed doped Mo/Nb thermocouple corrected for furnace temperature instability assessed with a Type-S thermocouple.

It shows no clear tendency of the thermocouple to stabilise though the drift is less important after 100 h of annealing. The situation was however better with the alumina-sheathed thermocouples. This kind of drift has already been reported by Villard *et al* [14] with a non-doped Mo/Nb thermocouple and several possible reasons were assumed, like mechanical stress, material oxidation etc.

It is worth noting that heat treatments at a similar temperature of 1100 °C were performed in the past at Thermocoax during periods of time exceeding 2000 h and have on the contrary shown that the thermocouples tend to stabilise quite rapidly (less than 100 h in all cases) and the overall drift of the emf of the thermocouples was less than 10-15°C, over the 2000+ h [15].

The obvious different behaviours observed between these three heat treatment test results (at CEM, LNE and CNAM and Thermocoax) are unexplained so far. The possible reasons could be the nature of the wires, if it has evolved over time or the occurrence of a contamination or structural damages during the preliminary tests and the measurements at the silver fixed point and/or in the oil bath.

It is therefore essential to perform further research on these thermocouples, or similar types, in the future and to define the most suitable thermal annealing procedures.

3.1.2.2 Practical Acoustic Thermometry

Operating for a prolonged period in an intense radiation environment places demands on all measuring apparatus, but the demands on temperature-measuring equipment are among the most extreme.

The reason is that the temperature-dependent properties of a thermometer typically depend on fine details of the electronic and mechanical structure of the thermometric material. When placed into a high-radiation environment these details are easily affected and the thermometer immediately begins to drift from its calibrated state. Thus it is desirable to choose a thermometry technique which has the possibility of *in situ* calibration; has a thermometric material which is insensitive to radiation; and is based on well-understood physics and engineering principles. Practical Acoustic Thermometry (PAT) satisfies all these requirements.

a- Principle of operation

The inference of temperature is based on a measurement of the speed of sound in a gas – typically argon. This link is robust and simple, stemming from the relationship between temperature and the speed of sound in a gas, and is the basis of the most accurate temperature measurements ever made [16]. In these measurements the frequencies of acoustic resonances within highly-perfect spherical cavities are measured.

In PAT we abandon resonator-based measurements and instead measure the speed of sound by a time-of-flight technique. The key to the practicality of the measurement is to time the speed of an acoustic pulse along an acoustic waveguide: a tube.

Importantly the tube can be made of any material: plastic, metal, or ceramic. Its function is simply to guide the sound to the region of thermometric interest. Thus for high-radiation environments devices can be manufactured from any engineering material capable of surviving the environment of interest. The tube may be bent or formed into complex shapes with negligible effect on sound transmission, guiding sound in a similar way to the guiding of light by an optical fibre.

The absorption of sound occurs within the thermal and viscous boundary layers at the inner perimeter of the tube. These boundary layers are typically ~0.01 mm and for tubes with a diameter more than a few millimetres, losses are low. For example, for tubes with an internal diameter of 6 mm at room temperature, the absorption of sound with a frequency of 100 Hz is characterised by a 1/*e* absorption length of 7.6 m. This property makes it possible to position loudspeakers and microphones outside the intense radiation environment, thus allowing for periodic replacement, servicing and upgrading.

b- Local or average temperature

In its simplest construction a PAT device is sensitive to the average temperature along the length of the waveguide. For many applications this is exactly what is required. For example, if the average temperature of coolant in a pipe is required, then by running a waveguide in a loop through the temperature field, the transit delay can automatically average the temperature.

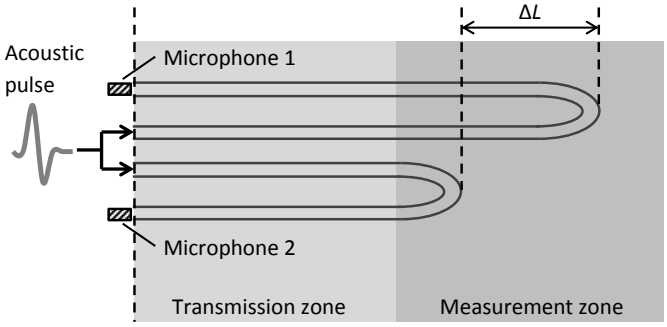

Figure 11. Schematic of a two-tube PAT thermometer. By finding the difference in transit times in the two tubes, the time taken for the sound to travel the length ΔL can be deduced and so the local temperature can be estimated.

But for many applications it is also important to localise the region over which the device is sensitive. This may be achieved in many ways, but typically two tubes of different lengths are used (Figure 11). Alternatively a single tube with a change in diameter may be used.

c- Performance

Figure 13 shows the performance of a PAT device made from two silica tubes 1 metre in length with a 20 cm length exposed to the central heated zone within a uniform three-zone furnace. Based on a single calibration of the device at 20 °C; the deviations from a calibrated Type R thermocouple amount to less than 2 C, over the entire range up to 1000 °C. This level of agreement arises because the thermal expansion of the silica tube is small ~0.5 × 10^{-6} °C^{-1} and so can be adequately compensated. So although silica is inappropriate for the construction of practical engineering devices, this result indicates that our theory [7] must be substantially correct.

Figure 14 shows the performance of a PAT device made from two Inconel tubes; again based on a single calibration at 20 ^{o}C, the deviations from a calibrated Type R thermocouple amount to $\Delta T \approx 13$ C at 1000 °C.

Iconel was chosen as it should be a material suitable for practical engineering devices. However, the reason for the larger error is that the thermal expansion varies from one batch of Inconel to another and so cannot be corrected without specific knowledge of the Inconel batch. But if the deviations are fitted with a quadratic polynomial – equivalent to calibrating at 1000 °C – then temperatures errors are on the order of 2 °C at 1000 °C.

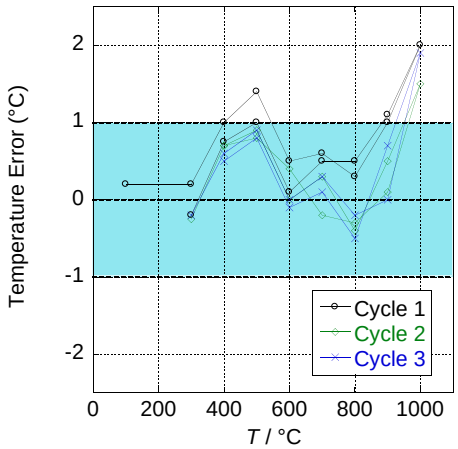

Figure 13. The temperature error of a PAT device made of silica compared with a calibrated Type R thermocouple over three heating cycles from 20 °C to 1000 °C. The predicted temperature is based entirely on a single calibration at 20 °C. The shaded band shows a range of ±1 °C.

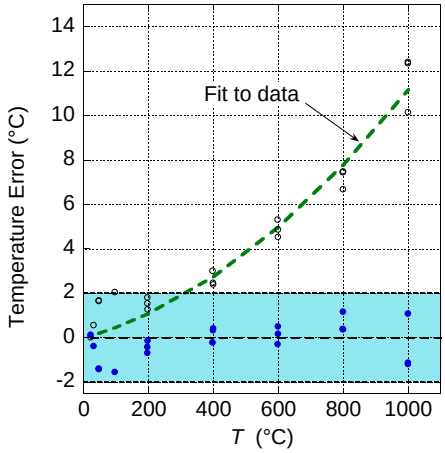

Figure 14. The temperature error of a PAT device made of Inconel compared with a calibrated Type R thermocouple. The 13 °C error at 1000 °C is because the thermal expansion of the Inconel has not been compensated for correctly. If instead of a single calibration at 20 °C the device were calibrated like a conventional sensor, then errors would be likely to lie within ± 2°C.

Conclusion and prospects

This project has allowed, in a short time frame, the realisation and characterisation of a series of solutions that can be used in the nuclear industry field. The Fe-C fixed-point was extensively studied and traceable temperatures have been assigned to the eutectic solid-liquid transition. This point is now made available for post-irradiation studies or calibration services [18]. Self-validation techniques have been trialed with success and will probably have multiple applications in the future. Tests of the Mo/Nb thermocouples have revealed challenges with significant drifts in the temperature measurement with time. Practical acoustic thermometry was shown to work reliably in range 20 ^{o}C to 1000 ^{o}C and will hopefully work at even higher temperatures with the use of durable metals. It is believed such a thermometer is capable of operating for decades in regions of intense irradiation.

As for the future developments and a possible continuation of this project, we believe safety requirements will be stricter after the recent accident in Fukushima. Temperature sensors have to prove even further reliability and stability on the long term as well as the ability to deliver signals close to, or even above, the limits of their specifications in term of temperature range in particular. One of the lessons learnt from Fukushima is that safety-related instrumentation should still be usable in case of accident to give information as long as possible [19]. Therefore there is a need in developing and characterising remote instrumentation for traceable temperature measurements, among other physical quantities, in reactors which could be in particular monitored from distant control stations to reduce the risks.

3.2 Improved thermochemical data and modelling for nuclear design

A number of designs for Generation IV reactors are currently being considered; all of them will operate at relatively high temperatures (i.e. above 1000 ^{o}C) and there will be a deliberate aim to keep decay and transmutation products within the fuel to limit its potential as a source of weapons grade material. Modelling will be a key component in the design of any new nuclear installation. One aim in the project was the development of new data for the nuclear fuel and its interaction with the coolant, containment materials and the environment that was previously not available. Before design and commissioning of a new nuclear facility it is necessary to understand completely all aspects concerning safety. One of the aspects which must be considered is the potential effect of release of nuclear fuel and fission products into the environment and its chemical interactions with the atmosphere, coolant and containment materials. This understanding cannot be achieved solely on the basis of experiment as this would be too hazardous and costly. A more flexible and ultimately more reliable approach is to use materials modelling and particular thermodynamic modelling in carrying out calculations relating to potential accident scenarios. This approach requires access to critically assessed thermodynamic data for all the phases and species which could be formed. Thermodynamic data and phase diagrams were critically assessed in the project to enable modelling of the potential interaction between a sodium coolant and both the nuclear fuel containment materials and atmosphere of a sodium cooled fast reactor.

3.2.1 The calculation of Phase Equilibria

The principles behind the calculation of chemical and phase equilibria are now well established and these have been implemented in a wide range of software products. Underlying all of these products is the principle that thermodynamic properties for multicomponent systems can be estimated from critically assessed data for their component systems e.g. pure components, binary systems etc. using well tested, reliable thermodynamically consistent models. The models used may be different for each type of phase to reflect the known structure of the material. For example the thermodynamic properties of a gas phase are calculated as the weighted sum of the Gibbs energies of the species with an extra term arising from ideal mixing of the gas phase species. However, the thermodynamic properties of a crystalline phase exhibiting a range of homogeneity on a variety of sublattices are based on data for a number of ideal compositions where each sublattice is filled with one particular element. Again an ideal entropy term and, in this case, a non-ideal, 'so-called' excess, term are included to model the variation of the thermodynamic properties with mixing of the elements on the sublattices.

For each of the component systems all the potentially diverse experimental data e.g. enthalpies of mixing, partial pressures, heat capacities, thermal arrests, microstructural information, are used together to generate a small set of coefficients for thermodynamic models which represent and reproduce all of the experimental information. Inevitably for some systems of interest there may be no or very little experimental information available. In such cases it may be necessary to estimate missing parameters from experimental results for similar systems or to calculate key properties using ab-initio quantum mechanics. The use of quantum mechanics for the calculation of structure and thermodynamic properties of simple gaseous molecules and crystalline materials is well established and is available in commercial and non-commercial codes.

It is vital when dealing with chemical thermodynamic properties to use a consistent reference state for all the components. Failure to do so will inevitably lead to incorrect results when calculating chemical or phase equilibria. The most common reference state for the Gibbs energy is known as the Standard Element Reference (SER) which is based on the enthalpy of the pure elements in their defined reference phase at 298.15 K (denoted as G-HSER), normally the phase stable at 298.15 K and 100 kPa, coupled to the absolute entropy. The data most commonly used for the different phases of the pure elements have been published by Dinsdale.

The models for the representation of the thermodynamic properties of the various phases as functions of temperature and composition are embodied in software packages which also include facilities for the calculation of equilibria between phases by minimising the Gibbs energy for a specific composition by varying the compositions and amounts of the competing phases. Ultimately phase diagrams can be calculated by systematically following phase boundaries across temperature, pressure and composition space.

3.2.2 Use of phase diagram calculations for simulating behaviour of nuclear fuel

Within the project the main thrust of the data assessment activity was concerned with the development of critically assessed data that would represent the potential interaction between the sodium coolant and the MOX nuclear fuel. Data for the fission products and containment materials have also been reviewed and new data assessed to represent the interaction between them, the Na coolant and the environment, in order to permit the calculation of phase and chemical equilibria for severe accident scenarios. Although data have been assessed or validated for a range of systems two systems are highlighted below.

A. Thermodynamic data for Na-I system

In a nuclear accident it may be possible for the sodium coolant in a sodium cooled fast reactor to come in contact with the fuel and decay products. One such product could be iodine and therefore it is necessary, in order to develop a comprehensive database, to derive accurate thermodynamic properties for the Na-I system over a range of temperatures and compositions. The system is characterised by a miscibility gap in the liquid phase closing at 1033°C (1306 K) and a stoichiometric compound, NaI, melting congruently at 660.1°C (933.2 K). The gas phase is generally recognised to be well described in terms of NaI, Na_2I_2 species in addition to those for the elements Na, Na_2, I, I_2. The thermodynamic properties of the crystalline phase have been fairly well studied as summarised by Cordfunke and Konings. In principle the thermodynamic properties of the liquid phase could be represented adequately with variation of composition by a number of different models. However, because these data should be capable of being used in combination with other similar datasets to represent the thermodynamic properties of the liquid phase with many more cations and potentially more anions, the best approach is to choose a model with some physical basis taking account of

the charge on the ions, which nevertheless offers flexibility to extrapolate into regions where no experimental data are available and supports the introduction of extra components and species. The most convenient model is therefore one which assigns different sublattices to the cations from those of the anions e.g.

(Na^+) (I^-, Va^-)

where the charged vacancy of the anion sublattice allows the composition to vary between pure Na and NaI. If it were desired to extend the description to cover the composition range to pure iodine it would be possible to introduce positively charged vacancies on the cation sublattice.

For this description the Gibbs energy of a composition x_{Na}, x_I in the liquid phase at a temperature T, is given by:

$$G = y_I\, G_{NaI} + y_{Va}\, G_{Na} + R\, T\, (y_I \ln(y_I) + y_{Va} \ln(y_{Va})) + G_{excess}$$

Where G_{Na} and G_{NaI} are the Gibbs energies of pure Na and NaI, y_{Va} and y_I are the site fractions of vacancies and iodine ions respectively on the anionic sublattice. R is the universal gas constant and T the temperature in kelvins. G_{excess}, the excess Gibbs energy derived from a critical assessment of the experimental data, is given by:

$$G_{excess} = y_I\, y_{Va}\, ((69823\text{-}37.3921\, T) + (-2708.7\text{+}.0196034\, T)\, (y_I - y_{Va}))$$

The figure below shows the phase diagram calculated using thermodynamic data generated for this model with the experimental data superimposed. The agreement with the experimental phase diagram information is very good and indicates that the assessed data can be used with confidence as a basis for calculations of phase equilibria in more complicated systems.

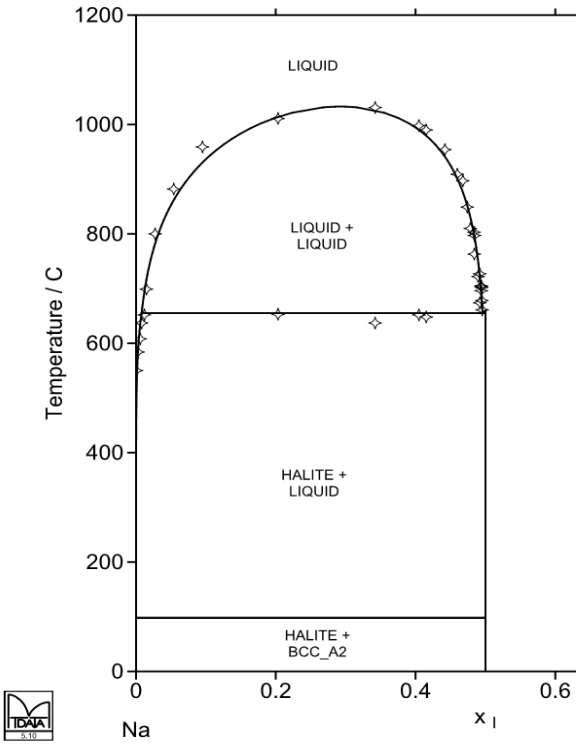

Calculated phase diagram for the Na-I system with experimental data superimposed

An understanding of the thermochemistry of the Na-I system is technologically important not just for the nuclear industry. High power, high efficiency lighting systems also utilise molten salt systems involving NaI often in combination with a rare earth iodide. This is quite typical in thermodynamics where data for a particular simple system may have great importance in a number of different technological areas. As mentioned, NaI vaporises to both monomeric and dimeric forms. Although this is well known the ratio between the two species in the vapour is still quite unclear although it is quite important technologically. There have been several attempts to clarify the equilibrium between the two species and thus to tie down

their thermodynamic properties but ultimately further experimental data are still required. More recently Ohnesorge has carried out measurements by Knudsen Cell Mass Spectrometry. An alternative method to derive thermodynamic properties for the monomer and dimer would be to use ab-initio quantum mechanics in order to derive the enthalpy of formation of the two species, and hence the enthalpy of dimerisation. Such techniques are already used widely to calculate the properties of the molecules, such as bond distances, angles, vibrational frequencies, which, with spectroscopic information, allow the calculation of the heat capacity of the gas phase species and the entropy of the species at 298.15 K. The following total enthalpies have been calculated relative to the nuclei and electrons using a B3LYP/SDD functional :

2NaI(g) : −912528.469 kJ mol^{-1}

Na_2I_2(g) : −912687.550 kJ mol^{-1}

The difference between these two very large values gives an enthalpy of dimerisation of −159.1 kJ mol^{-1} which should be compared with an assessed value based on experiment of −175.6 kJ mol^{-1}. As mentioned earlier this value is uncertain. Although the agreement between these two values in normal thermochemical terms would not be considered good, this result actually indicates that the ab-initio calculation of the total enthalpy is effectively accurate to better than 0.002 %.

B Thermodynamic data for the Na-O system

A thermodynamic assessment of the Na-O phase diagram was completed to understand the phase equilibria which are established after the interaction between sodium and oxygen. Four intermediate compounds were isolated, the oxide Na_2O, the peroxide Na_2O_2, the superoxide NaO_2 and the ozonide NaO_3, the latter two being unstable under ambient conditions. Therefore, they do not appear in the equilibrium phase diagram shown below. Sodium oxide can be prepared by reaction of metallic sodium with deficit amount of oxygen, but the yield is normally not very high. Hence, it is very difficult to isolate Na_2O in a pure form. Burning sodium metal in oxygen gives peroxide, while superoxide can be prepared in autoclave under high pressure of oxygen and elevated temperature (~300 °C).

A critical review of the thermodynamic properties of the elements and the intermediate compounds was completed and the selected data was used for the assessment of the Na-O phase diagram. The data for Na and O_2 end-members was taken from the review of Dinsdale, the data for Na_2O from thermodynamic tables by Barin, while the data for Na_2O_2 were taken from thermodynamic tables of Knacke et al.

No solid solution is found in the Na-O system, thus the only solution treated in the current assessment was the liquid phase and the gas phase. The gas phase was treated ideally considering the following gaseous species: Na(g), O_2(g), NaO(g), NaO_2(g), Na_2O(g), O(g), Na_2O_2(g) and O_3(g). The liquid phase was described by two sublattice ionic liquid model of the general scheme:

$$\left(Na^{+}\right)_P\left(O^{2-}, Na_2O_2, Va^{Q-}, O\right)_Q,$$

in which P and Q are the stoichiometric coefficients with Q = 1, while to maintain the electroneutrality P is calculated according to:

$$P = 2 \cdot y_{O^{2-}} + Q \cdot y_{Va^{Q-}}.$$

The y-terms in the above given equation correspond to molar fractions of electro-negative species. Based on the selected scheme, the cationic sublattice contains monovalent sodium cation only, whereas on the second sublattice oxide anion mixes with neutral species of sodium peroxide and oxygen and with charged vacancy. The end-members of the thus defined liquid solution are liquid Na, liquid ½O_2, liquid Na_2O and liquid Na_2O_2.

The excess Gibbs energy of the Na-O liquid solution is related to the interactions on the anionic sublattice between various species with the general equation defined as:

$$\Delta G^{xs} = y_{O^{2-}} y_{Na_2O_2} \sum_{i=0}^{n} L^i (y_{O^{2-}} - y_{Na_2O_2})^i + y_{O^{2-}} y_{Va^{Q-}} \sum_{i=0}^{n} L^i (y_{O^{2-}} - y_{Va^{Q-}})^i + y_{O^{2-}} y_O \sum_{i=0}^{n} L^i (y_{O^{2-}} - y_O)^i$$

$$+ y_{Na_2O_2} y_{Va^{Q-}} \sum_{i=0}^{n} L^i (y_{Na_2O_2} - y_{Va^{Q-}})^i + y_{Na_2O_2} y_O \sum_{i=0}^{n} L^i (y_{Na_2O_2} - y_O)^i + y_{Va^{Q-}} y_O \sum_{i=0}^{n} L^i (y_{Va^{Q-}} - y_O)^i$$

The L^i terms in the equation are parameters to be optimised and are written in general polynomial form:

$$L^i = A + BT + CT\ln T + DT^2 + ...$$

The assessed parameters obtained in this study are listed below:

$$L^0_{(Na^+)_P(O^{2-},Na_2O_2)_Q} = -21500$$

$$L^0_{(Na^+)_P(O^{2-},Va^{Q-})_Q} = 91000$$

$$L^1_{(Na^+)_P(O^{2-},Na_2O_2)_Q} = 22000$$

$$L^2_{(Na^+)_P(O^{2-},Na_2O_2)_Q} = -53000$$

$$L^0_{(Na^+)_P(Na_2O_2,O)_Q} = 1250$$

$$L^1_{(Na^+)_P(O^{2-},Na_2O_2)_Q} = -11000$$

The optimisation of the Na-O phase diagram was based on selected experimental data of oxygen solubility in liquid sodium published by Noden and the equilibrium data reported in by Bouaziz et al., Tallman and Margrave and Bunzel and Kohlmeyer. The assessed phase diagram is shown below. Two compounds are stable in the Na-O system, the Na_2O oxide which undergoes two allotropic transitions in the solid state ($T_{tr.1}$ = 1023 K and $T_{tr.2}$ = 1243 K) and melts congruently at 1405 K and the Na_2O_2 superoxide, which has one transition in the solid state ($T_{tr.}$ = 785 K) and decomposes at 950 K forming liquid and oxygen. Furthermore, a eutectic equilibrium is found in the region between the oxide and peroxide at T = 841 K and x(O) = 0.468. The congruent boiling point of the liquid solution is found at T = 2080 K and x(O) = 0.340.

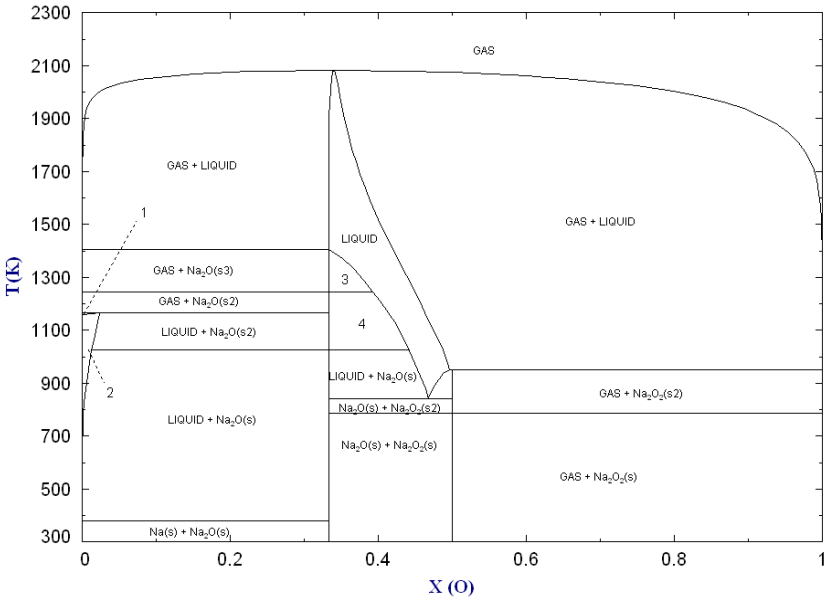

Calculated Na-O phase diagram. Numbered phase fields:

1 – GAS + LIQUID; 2 – LIQUID; 3 – Na_2O(s3) + LIQUID; 4 –Na_2O(s2) + LIQUID.

Conclusions:

Ultimately phase diagrams for simulating behaviour of nuclear fuel were calculated by systematically following phase boundaries across temperature, pressure and composition space. MTDATA [19] was used in the work reported here both in terms of the calculation of phase equilibria and through use of its Assessment Module, which provides facilities for the derivation of the critically assessed coefficients referred to above

from experimental thermodynamic and phase diagram data. The new data will be included in the next edition of MTDATA and a revised version of “Thermochemical data for reactor materials and fission products“.

3.3 Thermophysical properties of advanced materials

To improve the efficiency of proposed new reactors, they are required to operate at higher temperatures than the current generation. These high working temperatures induce metrological problems in relation with the selection of the most appropriate materials to safely construct reactors. Therefore, reference facilities at NMIs for the measurement of thermophysical properties (thermal diffusivity, normal spectral emissivity and specific heat) of solid materials up to 1500 °C or 2000 °C depending on the thermal properties were developed and improved. They were then applied to the thermal characterisation at high temperature of some materials that could be used by nuclear research laboratories to ensure the traceability to the SI of their thermal properties measurements, particularly for materials used in the design of generation IV reactors.

3.3.1 Development and improvement of reference facilities

The metrological reference diffusivimeter of LNE was limited to 1400 °C for the study of homogeneous solid materials; therefore it was modified in order to increase its measurement capabilities up to around 2000 °C. To do this, an induction furnace suitable to the measurements of thermal diffusivity at very high temperature was specifically designed. This furnace, mainly composed by an enclosure cooled by water in the centre of which an inductive coil and a graphite susceptor are placed on a vertical axis, was fitted to the existing diffusivimeter of LNE (cf. Figure 15b). All the elements (IR detectors, pyrometers, mirrors, lenses, vacuum pump, etc.) needed for the adaptation of the LNE diffusivimeter to higher temperature measurements were also assembled (cf. Figure 15a). Their adjustments and settings were then performed in order to optimise the “quality” of measurements (signal to noise ratio in particular)

a) General view

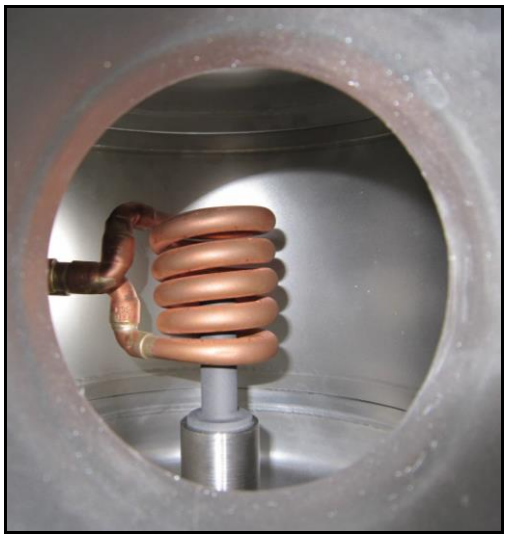

b) Graphite susceptor and inductive coil

Figure 15: LNE facility for the thermal diffusivity measurement of solids up to 2000 °C

Two complementary set-ups based on two different metrological approaches were developed by PTB and LNE for the measurement of normal spectral emissivity of solid materials at high temperature. The directional spectral emissivity $\varepsilon_\lambda(\lambda,T)$, at wavelength λ and temperature T is a dimensionless quantity, and is for a thermally radiating specimen defined as the ratio of the spectral radiance $L_{\lambda,\mathrm{Specimen}}$ of the specimen in a

particular direction to the spectral radiance of an ideal blackbody $L_{\lambda,\mathrm{BB}}$ at the same temperature T:

$$\varepsilon_\lambda(\lambda,T) = \frac{L_{\lambda,\mathrm{Specimen}}(\lambda,T)}{L_{\lambda,\mathrm{BB}}(\lambda,T)} \quad (1)$$

The method selected by PTB is based on a dynamic emissivity measurement using an adaptation of the laser flash technique. Its principle is given by the following relation, which states that the energy absorbed by the specimen (left hand term of equation 2) causes an increase of its internal energy (right side of equation 2).

$$\varepsilon_\lambda(\lambda,T)\cdot E_\lambda = m\cdot c_p(T)\cdot \Delta T(T) \quad (2)$$

If the specific heat $c_p(T)$ and the mass m of the specimen are known then its spectral emissivity $\varepsilon_\lambda(\lambda,T)$ can be determined by measuring the energy E_λ deposited by the laser pulse on its front face, and its increase of temperature ΔT. Figure 16 shows a general scheme of the apparatus (called ADεM) used by PTB for the dynamic emissivity measurement. It is based on a commercial laser-flash apparatus *Netzsch* LFA 427, which was greatly modified to measure both the laser pulse energy and the resulting temperature rise.

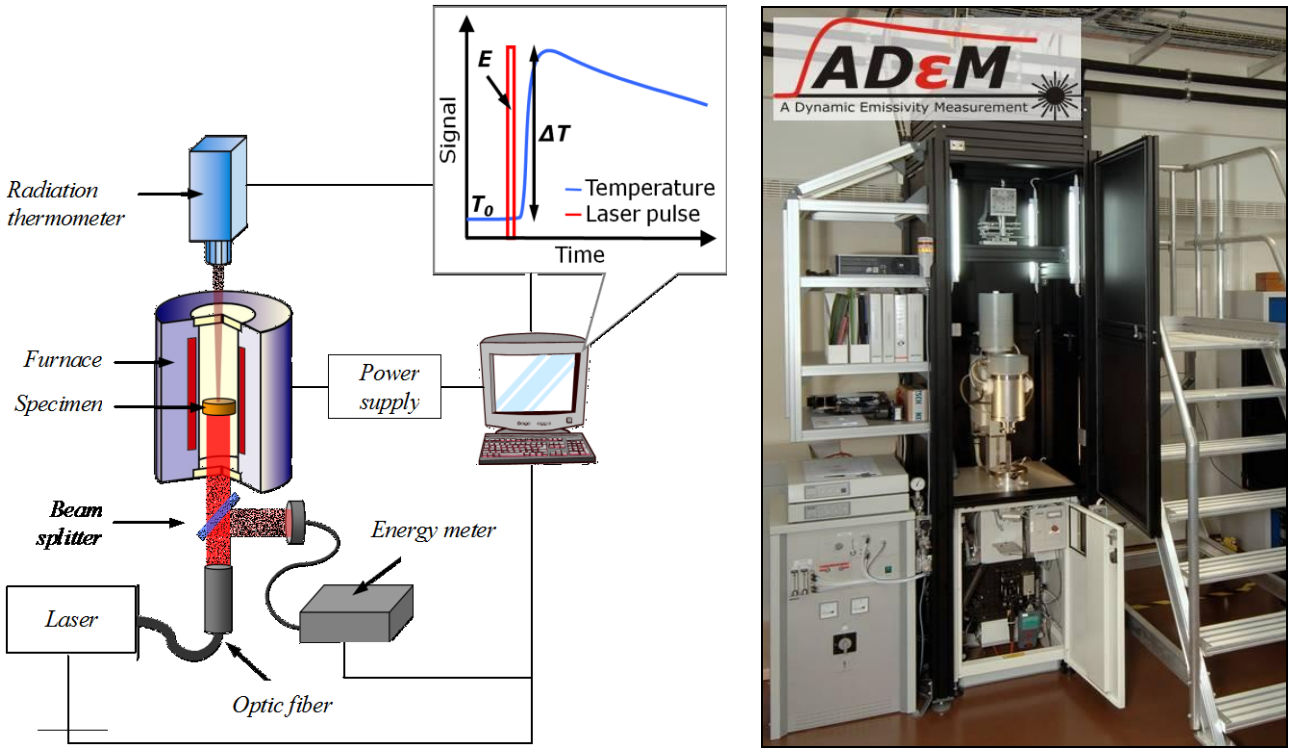

Figure 16: Scheme and picture of the reference apparatus of PTB for the dynamic emissivity measurement (ADεM)

LNE designed a new optical facility for measuring the directional spectral emissivity of solid materials up to 1500 °C in the spectral range from 0.8 µm to 10 µm with a spectral resolution of 1 cm^{-1}. The general principle of the technique is directly based on the definition of directional spectral emissivity (cf. equation 1), i.e. a comparison of the spectral radiance of the specimen at a temperature T to that of a reference blackbody at the same temperature.

A general view of the high temperature emissometer of LNE is presented on Figure 17.

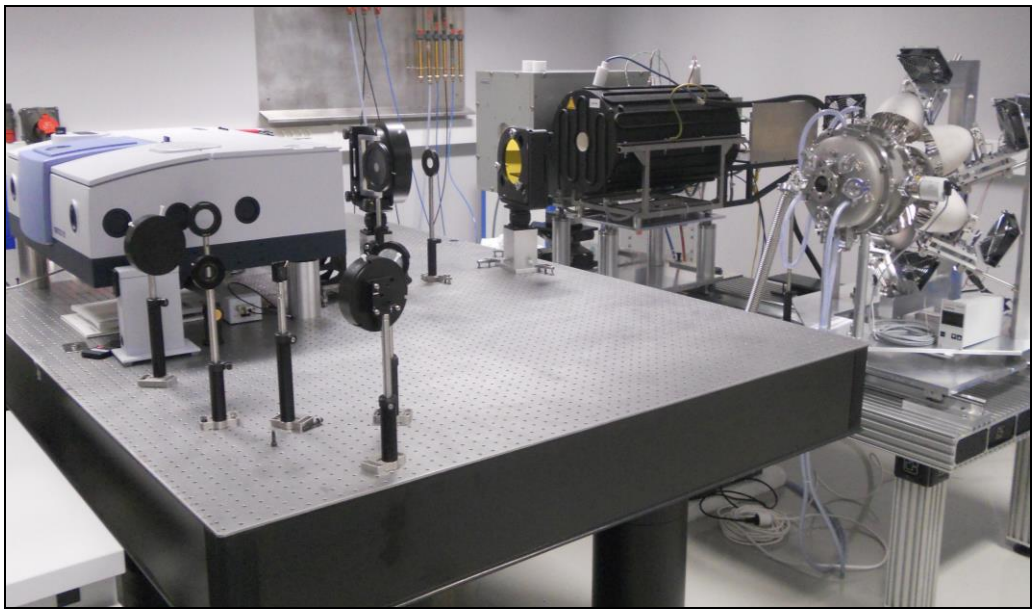

Figure 17. LNE facility for the spectral emissivity measurement at high temperature

Methods and calorimeters (Setaram Multi High Temperature Calorimeter) for the measurement of specific heat up to 1500 °C have been improved by NPL.

3.3.2 Application of the developed facilities to the thermal characterisation of a selection of solid homogeneous materials

The thermophysical properties of high purity 4N tungsten produced by *Plansee* and of isostatic graphite grade R6650P5 from SGL Carbon group were first measured at high temperature in order to perform the validation of the metrological facilities developed or modified in the first part of the project (section 3.3.1). The thermal characterisation of three other materials, which could be used as "transfer reference materials" for calibrating or validating equipment or methods used by nuclear research laboratories for the measurement of thermal properties at high temperatures, was then undertaken with these same facilities. Magnesium oxide (powder), nickel and zirconium dioxide (homogeneous solid materials) were selected because they are non-radioactive, stable at the temperatures of interest, and because of their relevance to thermal property measurements on nuclear materials (as investigated at JRC, e.g. UO_2, PuO_2, molten salts).

3.3.2.1 Thermal diffusivity

The thermal diffusivity of isostatic graphite, tungsten and nickel were measured over the temperature range 23 °C to 2000 °C by LNE with the high temperature diffusivimeter developed for this project, by NPL and PTB by using commercial apparatus (LFA 427 laser flash system), and by JRC with two laser flash setups (called LAF and CLASH) developed and built in-house for nuclear applications. The results are presented in tables I, II and III. Data in normal font refer to raw values while the data in italic are corrected values that take into account the thermal expansion of the tested materials measured at LNE and NPL by push rod dilatometry.

TABLE I : Thermal diffusivity of isostatic graphite

Thermal diffusivity (10^{-6} $m^2 \cdot s^{-1}$) - Isostatic Graphite								
Temperature (°C)	LNE		NPL		JRC		PTB	
	Raw data	Cor. data	Raw data	Cor. data	Raw data	Cor. data	Raw data	Cor. data
23	66.10	*66.10*	69.82	*69.82*		/	63.15	*63.15*
250	34.02	*34.09*	35.04	*35.11*		/	33.34	*33.41*
500	22.43	*22.54*	23.07	*23.18*	22.21	*22.32*	22.10	*22.20*
750	17.09	*17.22*	17.97	*18.11*	17.01	*17.13*	17.32	*17.45*
1000	14.45	*14.60*	14.92	*15.08*	14.01	*14.15*	14.53	*14.69*
1250	12.76	*12.93*	13.18	*13.36*	11.99	*12.15*	12.63	*12.81*
1500	11.66	*11.86*	11.75	*11.95*	11.69	*11.89*	11.32	*11.52*
1750	10.37	*10.59*	11.73	*11.98*	10.71	*10.94*	/	
2000	9.55	*9.80*	10.74	*11.02*	9.93	*10.19*	/	

Figure 18 plots the corrected values of thermal diffusivity of isostatic graphite versus temperature for the 4 laboratories. Values of LNE measured from 23 °C to 1400 °C with its reference diffusivimeter are given with uncertainty bars. Results obtained by LNE with the new diffusivimeter (red lozenges) and with the current reference bench (white lozenges) show a good continuity, with almost the same thermal diffusivity values measured at 1400 °C with the two configurations (12.24x10^{-6} $m^2 \cdot s^{-1}$ and 12.25x10^{-6} $m^2 \cdot s^{-1}$). Similar observations can be done with results of JRC measured with LAF and CLASH facilities.

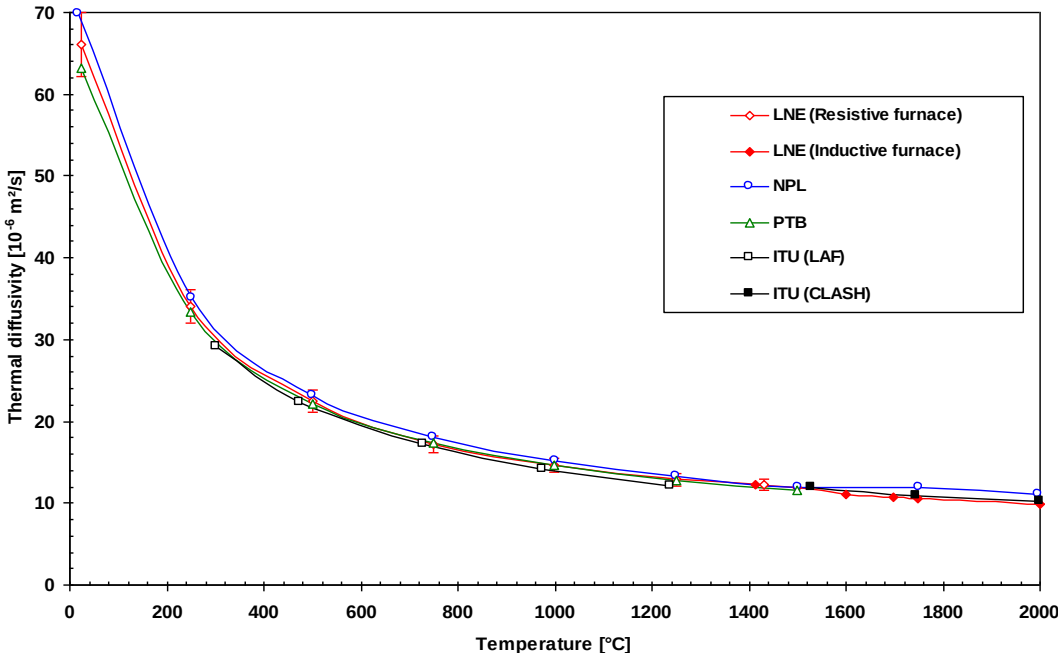

Figure 18: Thermal diffusivity of isostatic graphite as a function of temperature

Table II presents the thermal diffusivity values obtained by the four laboratories for the tungsten. Data interpolated from the recommended values of thermal diffusivity of tungsten given by Touloukian [1] are added in the last column. The differences among the results of laboratories are lower than 6 %, excepted at 1750 °C and 2000 °C. Data obtained for tungsten specimens are close to those recommended by [1].

TABLE II : Thermal diffusivity of tungsten

Thermal diffusivity (10^{-6} $m^2 \cdot s^{-1}$) - Tungsten									
Temp. (°C)	LNE		NPL		JRC		PTB		[1]
	Raw data	Cor. data	Raw data	Cor. data	Raw data	Cor. data	Raw data	Cor. data	
23	70.07	*70.07*	70.73	*70.73*	/		/		66.54
250	54.54	*54.64*	/		/		54.84	*54.94*	53.42
500	45.81	*46.00*	46.66	*46.85*	/		45.75	*45.94*	46.08
750	41.71	*41.98*	42.55	*42.83*	/		41.19	*41.46*	41.26
1000	38.93	*39.29*	39.72	*40.08*	/		38.33	*38.68*	37.85
1250	36.21	*36.64*	37.63	*38.07*	/		36.08	*36.51*	35.19
1500	33.94	*34.44*	33.17	*33.66*	34.88	*35.39*	34.17	*34.67*	33.02
1750	31.22	*31.78*	28.10	*28.61*	33.00	*33.59*	/		31.15
2000	29.02	*29.64*	24.08	*24.59*	31.58	*32.25*	/		29.60

[1] Y.S. Touloukian, R.W. Powell, C.Y. Ho and M.C. Nicolaou, "Thermophysical properties of matter, Thermal diffusivity", vol.10, IFI/PLENUM, New York, 1973.

The thermal diffusivities measured by LNE, NPL and PTB for the nickel from 23 °C up to 1200 °C were plotted in Figure 19 as a function of temperature. The results indicate good consistency between the measurements performed by the three laboratories with different apparatuses and estimation methods, and follow the same trends as data coming from [1].

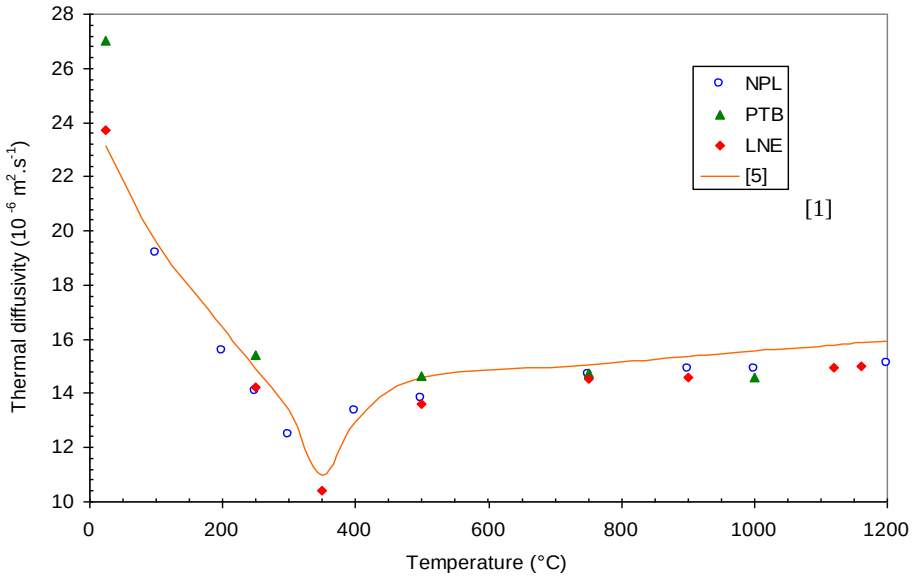

Figure 19. Thermal diffusivity of nickel as a function of temperature

3.2.2.2 Normal spectral emissivity

The normal spectral emissivity was measured under inert atmosphere from 750 °C to 1500 °C (every 250 °C) by LNE and PTB with the two complementary facilities developed for the project. Figure 20a shows the normal spectral emissivity of isostatic graphite measured by PTB at 1064 nm between 750 °C and 1500 °C by using the ADεM facility. These results are in good agreement with interpolated values from measurements performed by Neuer. Figure 20b plots the normal spectral emissivity of the graphite measured by PTB and LNE at 1250 °C for different wavelengths. The values obtained by PTB at 1064 nm and by LNE between 1500 nm and 3500 nm show good consistency and follow the same trend with wavelength.

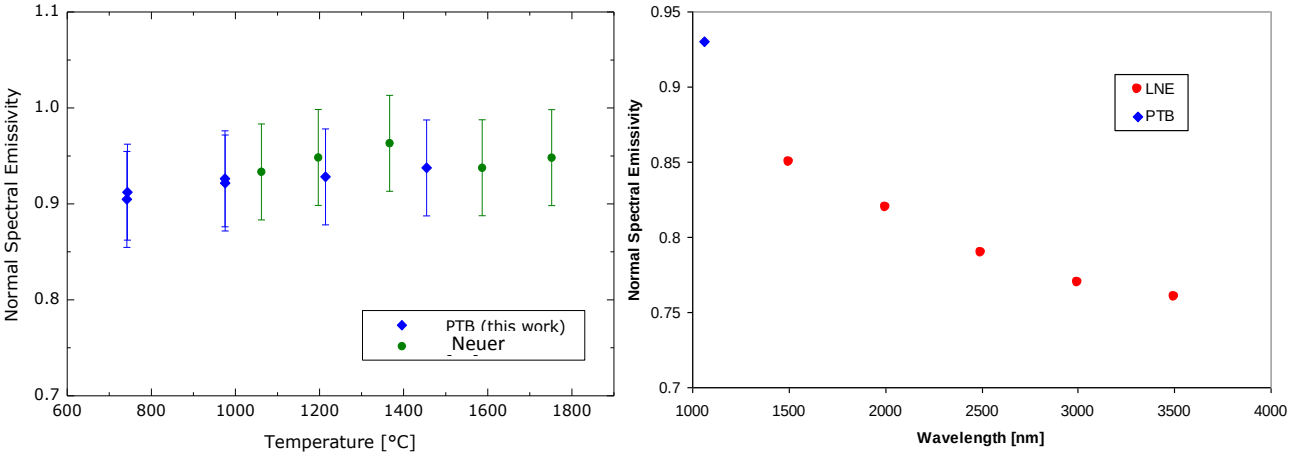

Figure 20. Emissivity of isostatic graphite

Normal spectral emissivity values measured as a function of wavelength on nickel specimens with the facility developed by LNE for the project are shown in Figure 21. These measurements were performed between 500 °C and 1200 °C for three consecutive thermal cycles. The variation of normal spectral emissivity of the nickel specimens with thermal cycling is due to a modification of the specimens during the tests. The surface condition has strongly evolved with roughness modification and grain growth (see Figure 22). Two other measurements were performed at 23 °C by LNE by using an integrating sphere reflectometer: one on the same specimen after the three thermal cycles, and another one with an as-received specimen. The two corresponding curves giving emissivity versus wavelength at 23 °C clearly demonstrate on Figure 21 the sensitivity of the normal spectral emissivity of these nickel specimens to the thermal cycling.

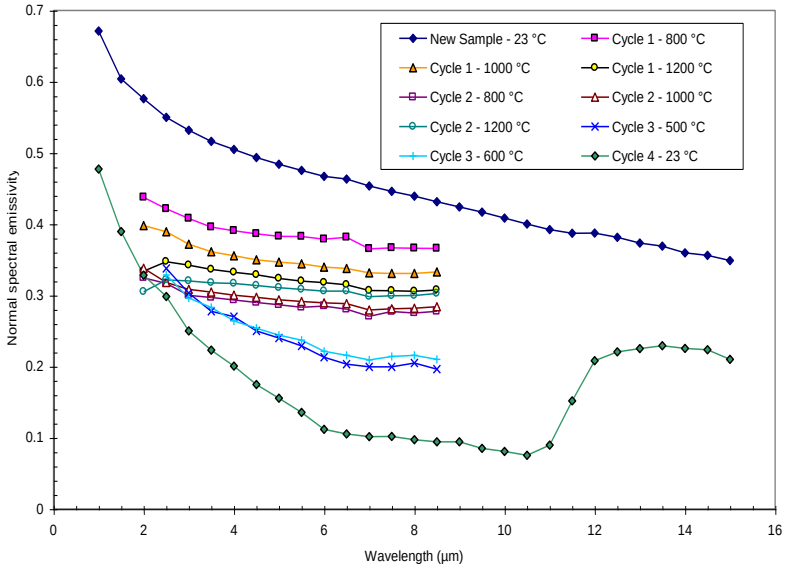

Figure 21. Normal spectral emissivity of nickel as a function of temperature and wavelength

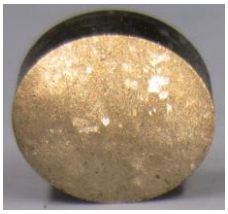

Figure 22. Specimen of nickel after test

3.3.2.3 Specific heat

Specific heat measurements were performed under inert atmospheres from 250 °C to 1500 °C every 250 °C in DSC mode by NPL and JRC by using Setaram MHTC-96 calorimeters. Results of specific heat measurements performed by JRC and NPL on isostatic graphite are presented in table III, and are compared with data issued from SGTE (Scientific Group Thermodata Europe) [2]. Repeated measurements performed by NPL during three successive heating cycles on the same graphite specimen give standard deviations lower than 4 % from 500 °C to 1250 °C and equal to 9 % at 1500 °C. The relative deviations between the measurements performed by JRC and NPL on the graphite with the same model of calorimeter (Setaram MHTC-96) but by applying two different scanning methods are between 4 % and 10 %.

TABLE III : Specific heat of isostatic graphite

Specific heat ($J \cdot g^{-1} \cdot K^{-1}$) - Isostatic graphite					
Temp. (°C)	JRC	NPL			[2]
250	1.103		/		1.264
500	1.671	1.519	1.600	1.584	1.627
750	1.759	1.686	1.758	1.741	1.813
1000	1.893	1.820	1.939	1.855	1.924
1250	1.976	1.966	2.124	2.061	1.997
1500	/	2.049	2.427	2.374	2.050

[2] A.T. Dinsdale, “SGTE data for pure elements”, *Calphad*, vol. 15, pp. 317-425, 1991

Results of specific heat measurements performed by JRC on tungsten and nickel specimens are presented in table IV, and compared with data from literature [2, 3]. Results of specific heat measurements performed by JRC and NPL on powder of magnesium oxide from 250 °C to 1250 °C are presented in table V, and compared with data from [4].

TABLE IV : Specific heat of tungsten and nickel

	Specific heat ($J \cdot g^{-1} \cdot K^{-1}$) - Tungsten		Specific heat ($J \cdot g^{-1} \cdot K^{-1}$) - Nickel	
Temp. (°C)	JRC	[2]	JRC	[3]
250	0.140	0.139	0.520	0.537
500	0.141	0.145	0.542	0.524
750	0.144	0.151	0.508	0.551
1000	0.158	0.157	0.525	0.588
1250	0.169	0.163	0.601	/

[3] P.D. Desai, “Thermodynamic properties of nickel“, *Int. J. of Thermophys.*, vol. 8, pp. 763-780, 1987

TABLE V : Specific heat of magnesium oxide

Specific heat ($J \cdot g^{-1} \cdot K^{-1}$) - MgO			
Temp. (°C)	JRC	NPL	[4]
250	1.242	1.069	1.142
500	1.245	1.086	1.220
750	1.196	1.128	1.266
1000	1.195	1.205	1.298
1250	1.328	/	1.328

[4] O. Knacke and O. Kubaschewski, "Thermochemical properties of inorganic substances", 2nd edition, Springer-Verlag, Berlin, 1991

Conclusion

The European metrological infrastructure in the field of measurement of thermo-physical properties has been improved and adapted to higher temperatures in order to provide reliable and traceable high temperature measurements for materials having thermal properties similar to those used in fission reactors. The availability of these accurate facilities and reference materials will improve the traceability of nuclear research laboratories measurements.

3.4 Improved cross sections through neutron metrology

The aim of this work was the improvement of neutron cross section measurement techniques in order to arrive at uncertainties as required for the design and safety assessment of new generation power plants and fuel cycles. These requirements are often very challenging, being at or beyond the state-of-the-art in neutron measurements, which is set by self-normalising methods and the neutron data standards used at laboratories where the data are measured.

3.4.1 Development of a secondary neutron fluence standard

The program of work included the establishment of an easy-to-use secondary fluence standard at one of the flight paths of the JRC neutron time-of-flight facility GELINA along with a procedure for reliable determination of the efficiency of fluence measurement devices used in neutron data measurements at JRC and elsewhere. The set-up consists of a fixed flux monitor, a reference chamber and a transfer chamber all mounted at the same neutron flight path of GELINA (see Figure 23).

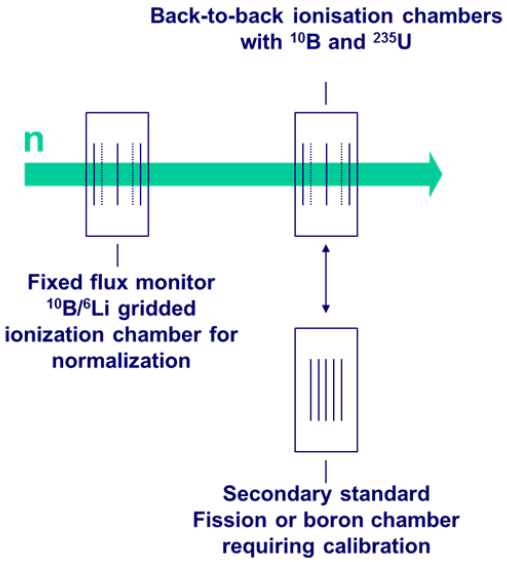

Figure 23: Schematic view of the set-up and procedure used to calibrate neutron fluence devices at one of GELINA's flight paths.

The flux monitor is mounted in the most upstream position and consists of a double Frisch-gridded ionisation chamber loaded with a ^{10}B layer and a ^{6}Li layer. The chamber is kept in position at all times and is used as a relative fluence monitoring device in order to register variations over time of the neutron flux at this particular flight path and in order to correlate measurements with different devices. The reference chamber consists of a double Frisch-gridded ionisation chamber loaded with a well characterised ^{235}U layer on one side and a ^{10}B layer on the other side (see Figure 24). The chamber is installed downstream from the flux monitor and permits determining the neutron flux as a function of neutron energy in an absolute way, by using the reference cross sections of ^{10}B and ^{235}U. The reference chamber can be replaced with any other fluence monitor in order to calibrate this device.

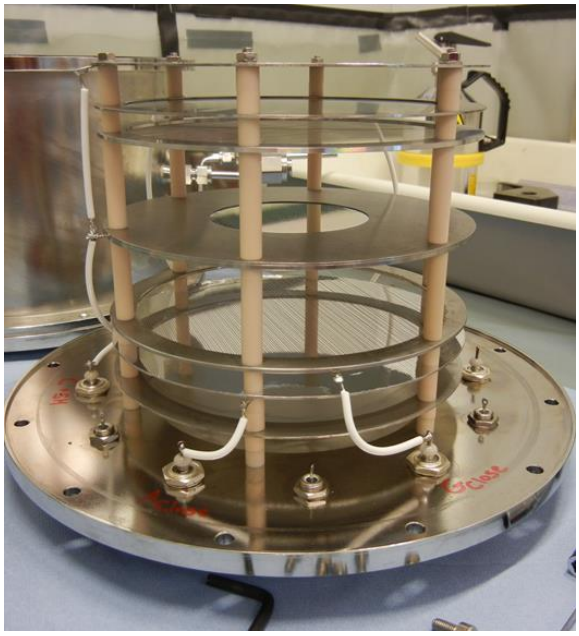

Figure 14: A double Frisch-gridded ionisation chamber loaded with ^{235}U and ^{10}B is used as a reference chamber for neutron fluence measurements.

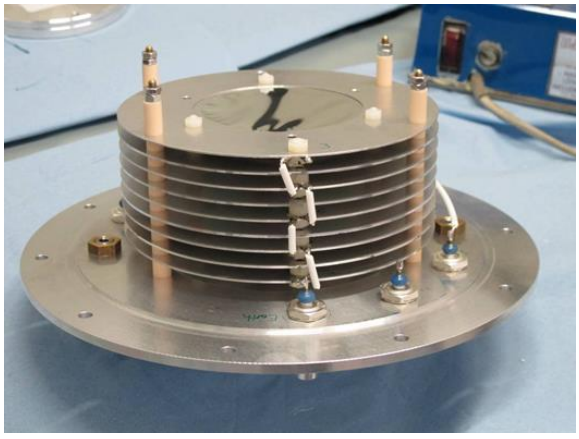

Figure 25: Multi-layer parallel plate chamber consisting of 8 layers of ^{235}U.

A multilayer parallel plate transfer chamber consisting of 8 layers of ^{235}U (see Figure 25).was calibrated using this method and used for fluence measurements at other neutron beams. All ^{10}B, ^{6}Li and ^{235}U layers were prepared by vapour deposition at the JRC (IRMM) target preparation lab. The ^{235}U layers were carefully characterised for their total areal density and their areal density distribution at using alpha particle counting in a limited and well-defined geometry. The neutron beam profile was determined using a Li glass based neutron camera. Both the areal density profile of the ^{235}U samples and the neutron beam profile were taken into account in analysing the detector response.

3.4.2 Applications

The potential of these fluence measurement devices was demonstrated by a number of neutron induced fission cross section measurements on ^{240}Pu and ^{242}Pu with mono-energetic neutron beams produced at two different NMIs, i.e. at the Van de Graaff accelerator and the cyclotron of PTB and at the Van de Graaff accelerator of NPL. The measurement were performed using gas filled detectors, consisting of a Frisch-gridded ionisation chamber containing the Pu sample, mounted back to back to a parallel plate chamber containing a ^{238}U sample. During the experiments the neutron fluence was measured in parallel with the ^{238}U parallel plate chamber and with the fixed neutron fluence monitors available at the respective institutes.

Conclusion

A secondary neutron fluence standard was developed and calibrated at the neutron time-of-flight facility GELINA of JRC. It consists of a flux monitor, a reference ionisation chamber containing a ^{10}B layer and a ^{235}U layer, and a parallel plate ionisation chamber with 8 well characterised ^{235}U deposits. These devices are used to determine the neutron fluence, based on the well-known neutron induced fission reaction on ^{235}U. All deposits have been prepared and characterised at the JRC (IRMM) target preparation lab. The secondary fluence standard at the GELINA facility can be used for reliable determination of the efficiency of fluence measurement devices used in neutron data measurements at the JRC (IRMM) and other national laboratories dedicated to measuring neutron cross sections. It is an essential tool to reliably calibrate fluence normalisation devices used in neutron time-of-flight cross section measurements to produce accurate neutron cross-sections essential to the nuclear power industry.

3.5 Improved decay data

Specific aspects related to the nuclear decay data improvement were high precision measurements of ^{238}U alpha-particle emission probabilities and experimental characterisation of the beta spectral shape using cryogenic detectors. These new measurements respond to user requests identified by the IAEA (International Atomic Energy Agency), according to the CRP F42006 (updated decay data library for Actinides).

3.5.1 Alpha spectrometry

In alpha-particle spectrometry one was faced with peculiar problems due to the extremely long half-life of ^{238}U. The low specific activity of the enriched uranium material required the use of relatively high amounts in the source, which was contradictory to the requirement of having a thin layer for optimum energy resolution. Months of research went into the production of sources by electrodeposition that could optimise between both requirements. An additional problem was the relatively short distance between source and detector to collect sufficient events for statistical accuracy. As a consequence, a significant amount of conversion electrons were detected coincidently with the alpha particles, leading to a distortion of the spectrum and wrong assignment of emission probabilities. In spite of mathematical corrections, measurements in different geometries lead to different results. This could only be solved by the design and implementation of a new magnet system to eliminate conversion electrons.

The work performed by JRC and CIEMAT led to the following conclusions: Source preparation by electrodeposition was optimised for uranium sources to yield good energy resolution for alpha-particle spectrometry. The thickness of alpha-emitting sources is preferably kept below 26 µg cm^{-2} to retain an energy resolution of about 15 keV. Mathematical corrections for coincidence effects with conversion electrons do not adequately compensate for the spectral distortion. The use of a magnet system eliminates conversion electrons and allows the determination of alpha emission probabilities with better accuracy and statistical precision. The accuracy of the alpha particle emission probabilities of ^{238}U could be improved by one order of magnitude compared to previously recommended values. The collaboration between JRC and CIEMAT was useful for finding solutions to the technical problems and for combining results which helped reduce the measurement uncertainty.

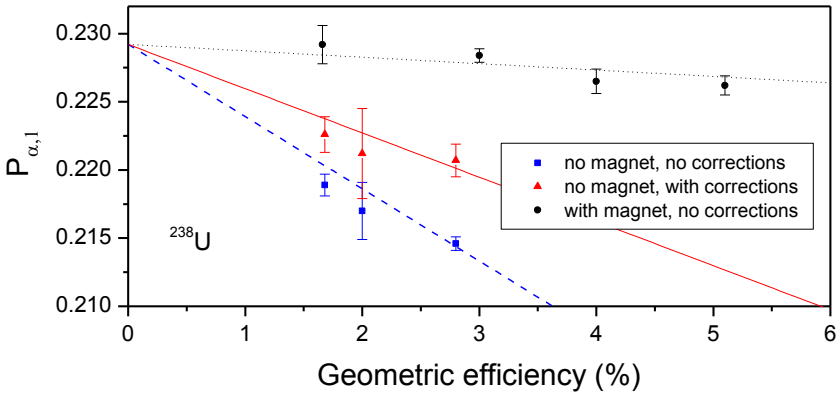

Figure 26. Emission probability values of the second largest peak in the alpha decay of ^{238}U, derived from the deconvolution of the spectra taken with magnet (circles) and without magnet, before (squares) and after (triangles) mathematical correction for coincidence effects.

3.5.2 Beta spectrometry

Beta spectrometry by means of a cryogenic detector is a novel technique that needed extensive testing to become operable. One of the problems encountered during the experiments was the dependence of the spectral distribution on the source production method. Tests with drop deposited sources were unsatisfactory: the measured spectra deviated from theory and from one another. It was found that the spectra resulting from electrodeposited sources were reproducible and closer to the theoretical spectrum. Still, there was a deviation from a standard calculation of the spectrum of an allowed beta transition, which could be solved by including the atomic exchange effect into the model. These measurements are a clear proof of the presence of exchange effects in beta decay and emphasise the need to account for them.
A cryogenic detector, more specifically a metallic magnetic calorimeter, was used for beta spectrometry firstly because of its high energy resolution and low energy threshold, and secondly because it was straightforward to produce a solid angle of 4π sr and high detection efficiency by enclosing the beta emitter in the detector absorber. Firstly, the spectrum of the pure beta emitter ^{63}Ni was measured. Then the first beta spectrum from a forbidden transition, ^{241}Pu, was measured. When including an exchange effect in the model, the measured spectral shape could be reproduced by theoretical calculation.

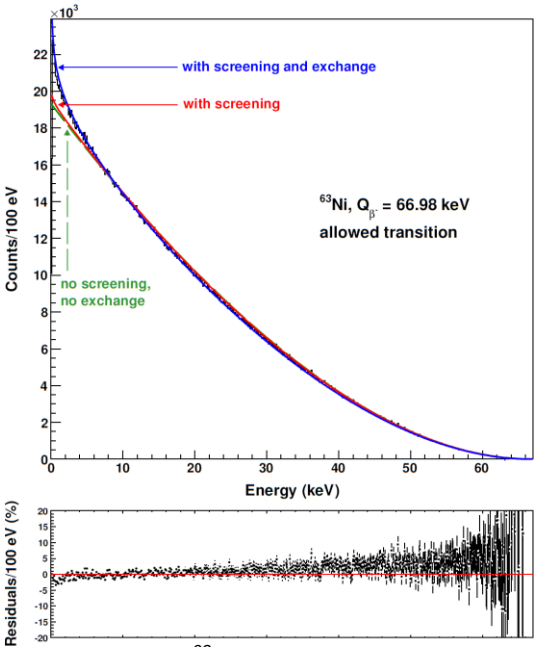

Figure 27. Beta spectrum of an electroplated ^{63}Ni source measured with a metallic magnetic calorimeter ("rugged" black line), compared with theoretical spectra without any correction for atomic effects, with screening correction and with screening and exchange effects. The lower part of the figure shows the residuals between experiment and the full theory including screening and exchange effects.

Conclusion

The alpha-particle emission probabilities of ^{238}U have been measured with high-resolution alpha-particle spectrometry. Sources were prepared of highly enriched ^{238}U material by electrodeposition. This was the result of a compromise between spectral resolution and counting rate. The measured emission probabilities agree within uncertainties with the previously published data but are significantly more precise. The new data are also more accurate owing to a better correction for true coincidence effects with conversion electrons.

The beta spectrum of ^{63}Ni was measured with several metallic magnetic calorimeters and different types of sources. The accurateness of the spectra measured with metallic magnetic calorimeters depends crucially on the quality of the source.

3.6 Measurement techniques for radionuclides - Triple-to-Double Coincidence Ratio

The Triple-to-Double Coincidence Ratio (TDCR) method in Liquid Scintillation counting (LSC) is a primary radionuclide standardisation method widely used in NMIs (for the standardisation of radioactivity/ Bq) and was primarily developed for the radioactivity measurement of beta emitters. It is based on liquid scintillation: the light is detected by three photomultipliers (PM) and the detection efficiency is evaluated by using a model which uses the ratio of triple-to-double coincidences between the PM tubes.

Currently, most TDCR systems were locally-made metrology instruments neither aimed at nor suitable for in-situ measurements. In this project, work was dedicated to the development of miniature self-calibrated primary TDCR systems, which are state-of-the-art, for use on-site. The challenge was to develop a versatile portable, table-top designed instrument, from this metrology device. This implied improvements for the miniaturisation of the detection chamber, for the miniaturisation of electronic modules by exploring the possibilities of digital treatment, and for the validation of models and extension of them to nuclides with special beta spectrum shapes, to nuclides with complex decay schemes including many gamma-rays and to nuclides with higher atomic number decaying by electron capture. Four prototypes of counters were built and validated by ENEA, CEA, NPL and PTB using various technical approaches.

3.6.1 The TDCR method in liquid scintillation counting

The LSC process is the emission of light following the interaction of ionising particles or photons with a liquid scintillator. The radiation–matter interaction eventually creates electrons, whose energy is dissipated within the solvent of the scintillator. Part of this energy is then transferred to the fluorescent molecules, which emit

light by radiative de-excitation. Depending on the nature of the scintillator, the light pulse may have a prompt component followed by delayed emission. The duration of the prompt emission is lower than 10 ns for most liquid scintillators.

The light emitted is generally in the blue to near-UV spectrum range. This emission is incoherent and isotropic, but most of the light escapes from the meniscus created at the scintillator–vial wall interface. The overall energy conversion in the liquid scintillation process is rather low: 1 keV of electronic energy produces only a few photons. Detection efficiency is thus generally lower than 1 and must be calculated.

The TDCR method is based on the free parameter model in LSC. Under some physical and statistical assumptions concerning the light emitted by the scintillator, the detection efficiency can be calculated from the knowledge of a free parameter linked to the intrinsic light efficiency of the scintillating source in a specific counter. The TDCR method is a way, among others, to calculate this free parameter. The basic physical and statistical models used are described hereafter.

If it is assumed that the energy *E* of an electron is released in the scintillator, light is emitted with a mean number of photons *m*. The statistics of the number of photons emitted by the scintillating source can be described by a Poisson distribution: the probability of the emission of *x* photons for a mean value *m* is

$$P(x/m) = \frac{m^x e^{-m}}{x!} \qquad (1)$$

These photons are collected on the photocathodes of the PM tubes and photo-electrons are then produced with a quantum efficiency □. The detection efficiency can be derived from the detection probability, which is the complement of the non-detection probability. The non-detection probability is the probability to get zero photo-electron for a mean expected value of *m*□.

When introducing this in the Poisson formula for a 1/3 symmetry counter using three photodetectors with the same quantum efficiency v, the detection efficiency for one photodetector is

$$R_1 = 1 - e^{-\nu m/3} \qquad (2)$$

This formula applies when the PM tube setting makes possible the detection of a single photoelectron.

For two and three photodetectors in coincidence, we get, respectively, Eq. (2) to the powers of 2 and 3. The detection efficiency for the logical sum of the double coincidences is:

$$R_D = 3(1 - e^{-\nu m/3})^2 - 2(1 - e^{-\nu m/3})^3 \qquad (3)$$

The light emission process is not linear and the mean number of photons emitted is known not to be proportional to the energy released in the scintillator by the ionising radiation. A semi-empirical relation, described by Birks, gives the mean number *m* of photons emitted as a function of the energy *E* released in the scintillator, and the linear energy transfer d*E*/d*x*:

$$m(E) = \int_0^E \frac{A\,dE}{1 + kB\dfrac{dE}{dx}} \qquad (4)$$

A is a free parameter characterising the LS-cocktail efficiency and *kB* is a semi-empirical parameter.

If the energy spectrum emitted by the radionuclide is described by a normalised density function *S*(*E*), the ratio of the probability of the triple coincidence to the probability of the double coincidence, *TDCR*, is:

$$TDCR = \frac{\int S(E)(1-e^{-\eta})^3 dE}{\int S(E)(3(1-e^{-\eta})^2 - 2(1-e^{-\eta})^3) dE}$$

with

$$\eta = \frac{\nu}{3}\int_0^E \frac{A dE}{1+kB\frac{dE}{dx}} \qquad (5)$$

This simple model assumes that the PMTs have similar efficiency but if this is not the case, a set of 3 equations must be solved instead of equation (5).

The triple and double coincidences are recorded by the LSC. For a large number of events, the ratio of experimentally determined counting rates converges towards the ratio of calculated efficiencies. The detection efficiency calculation algorithm is used to determine the free parameter *νA* (figure of merit as the number of photons emitted per unit of energy released in the scintillator), for which the experimental frequency ratio equals the calculated ratio. It can be shown that for pure beta spectra, there is a unique solution, but for other kinds of spectra, including those obtained for nuclides that decay by electron capture one TDCR value can correspond to up to three detection efficiency values. In that case, the use of several counting conditions for a single sample can solve the ambiguity.

3.6.2 General design principles and options

We adopted the following design principles, taking into account the constraints on the portability of the system and also the requirements of the TDCR model described above:

Portability and power supply; a portable TDCR system should fit into a standard car. If the counter is supposed to be handled by a single person, no part should be heavier than approximately 30 kgShielding; passive shielding is heavy and therefore reduces the transportability. An active shielding might lead to a loss of real counts, especially when measuring photon-emitting radionuclides. It might also influence the photon statistics, which is a crucial assumption of the TDCR model. Thus, a potential active shielding should be able to be disconnected. It also increases size and weight, and the evaluation of the guard detector signals complicates both the electronics and the software design.

Optical chamber and light collection; as the efficiency of the LSC process is low, it is very important to collect the maximum amount of light. As a rule, the uncertainty of the detection efficiency increases as the detection efficiency decreases, because the model has to correct for the missing information. It is advisable to use highly reflective materials in the optical chamber. Photodetectors choice and discriminator threshold adjustment; as the counter must have a non-zero detection probability for single photons, it is essential that the single-photoelectron peak is well resolved in order to allow a precise adjustment of the counter threshold. This implies the use of high-gain photodetectors having a good peak-to-valley ratio of the single-photoelectron peak.

Efficiency variation method; classical methods are based on optical (e.g. grey filters), mechanical (e.g. diaphragm or variation of the vial position) or electronic methods (e.g. PMT defocusing). Any efficiency variation method implemented in the counter increases size and complexity and hence could have an influence on the portability. Efficiency variation by means of chemical quenching is also possible and does not require special counter modifications.

Dead-time unit; prompt light emission is followed by afterpulses correlated to the initial emission. This results in pulse clusters and spoils the stationary nature of the observed process. Moreover, the noise of some photodetectors, like PMTs, can appear as burst of pulses and cannot be considered as stationary. It is thus necessary to add a dead time period after each detected event in order to avoid false coincidences of photocathode noise and delayed light emission. The base duration of this dead time is typically a few tens of microseconds.

System symmetry; the use of matched photodetectors in a symmetrical arrangement is the only design that permits the use of the simple TDCR model previously described. Nevertheless, as it is expected to have variability in the photodetector responses, it is necessary to have access to individual double coincidences and to use a TDCR model taking asymmetry into account.

Coincidence unit; considering that the prompt light pulse duration is less than 10 ns and that this pulse is followed by spurious after-pulses it is necessary to use fast detectors, fast preamplifiers and fast-coincidence units in order to acquire clean signals and to minimise false-coincidence corrections. An adjustment of the coincidence resolving time in the 20 ns to 200 ns range is desirable. The use of an FPGA-based system for digital pulse processing is desirable, as it is very flexible and may help to reduce the size of the system and to optimise its robustness. Asymmetries of the photodetector efficiencies must be taken into account [3] and at least the counting in channels AB, BC, AC and T must be recorded. Even if D can be deduced from the previous signals, its acquisition is interesting as it allows the verification of the fulfilment of balance equations. Other features, such as the counting of the single channels or gamma coincidences when using an additional gamma counter, can be considered as optional.

Detection efficiency variation methods; as for some nuclides, equation (5) might have several solutions, it is necessary to change the detection efficiency of the system to solve this ambiguity. The TDCR model also requires an external parameter: the *kB* coefficient. Several detection efficiency conditions give the possibility to find out the value of this *kB* coefficient for which the source activity remains the same for all counting conditions. Detection efficiency variation is possible by defocusing the photodetectors, by using coaxial grey filters around the source or by changing the position of the source in the optical chamber.

3.6.3 Description of prototypes

Each of the four project partners applied these design principles to develop their own prototypes which were:

ENEA counter

The optical chamber of the prototype developed by ENEA is made of PTFE, with a prismatic shape. The photomultiplier tubes used are Hamamatsu R7600U-200 square miniature PMTs, with a high quantum efficiency photocathode. The sample holder is composed of a lift to introduce the vial and there is an optical shutter to separate the sample holder and the optical chamber, so the PM tubes can be continuously powered, in order to increase the stability of the system.

Anode signals are directly processed by a CAEN digitiser, acting as level discriminator and fast ADC. The amplitudes of the pulses are recorded in a file, associated to timestamps, and the coincidence calculation is made off-line by software. This allows the possibility to reanalyse the measurement with different parameters like the coincidence resolving time and the dead-time type and duration. In practice, this off-line treatment is transparent, as the processing delay is a few seconds. More details on this instrument can be found in [20] and [21].

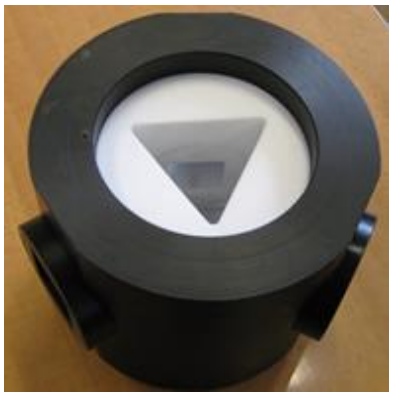

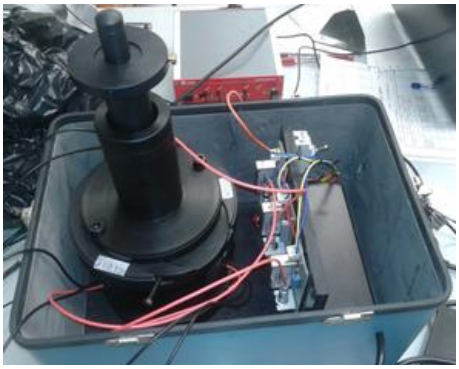

Figure 28. The optical chamber of the ENEA portable TDCR counter. Figure 29. ENEA TDCR counter

NPL counter

The optical chamber of the NPL prototype is made of aluminium, internally coated with a Spectraflect® reflective paint. The first PM tubes tested were 29 mm diameter ET 9142A but they were replaced by Hamamatsu R6095 28 mm diameter tubes with lower noise and better resolution of the single-electron peak. The system is equipped with piston type sample loading and an efficiency-varying system. The installation of an electrically-operated shutter is planned like the installation of a stepper motor to set the vertical position of the vial. Anode signals from the PMTs are amplified by Ortec 474 fast amplifiers and processed by the MAC3 coincidence unit [22]. More details on this instrument can be found in [23].

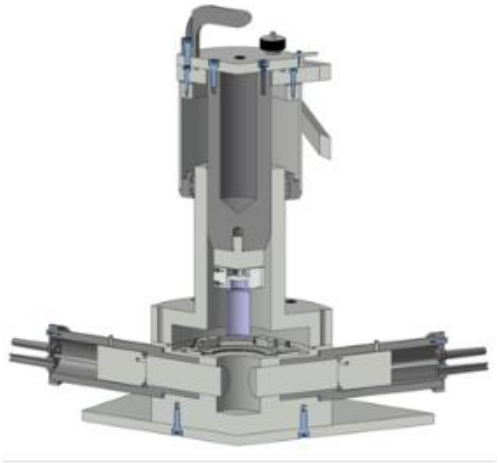

Figure 30. Internal view of the optical chamber of the NPL counter

Figure 31. Optical chamber of the NPL TDCR counter

PTB counter

The PTB prototype uses 3 channel PM tubes from Perkin Elmer, in an optical chamber made of highly reflective material, OP.DI.MA ODM98 from Gigahertz-Optik. The opical chamber and high-voltage modules are installed in a compact box. Signal processing is made by an FPGA-based coincidence module 4KAM, specifically developed by PTB. This module emulates the MAC3 module but with additional features like an adjustable coincidence resolving time, and includes counters for coincident and non-coincident information and time signals. The processing is made on-line and information is transferred to a personal computer through a serial interface. More information on this instrument can be found in [23].

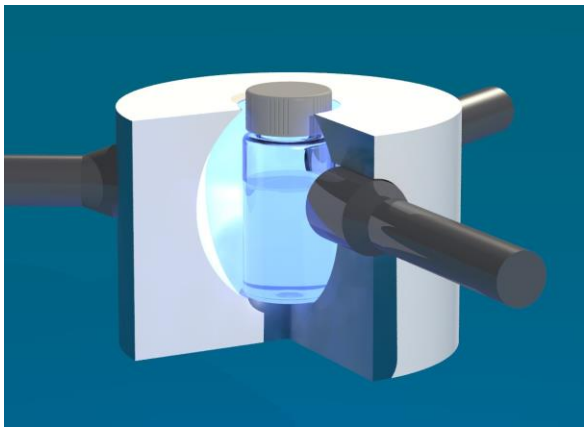

Figure 32 Artist's view of the optical chamber of PTB counter

Figure 33 The PTB TDCR counter with optical chamber, PM tubes and HV supplies.

CEA counter

The optical chamber of the CEA prototype is made of polymer coated with TiO_2 paint. Six PerkinElmer channel PM tubes are used which are operated two by two in parallel in order to increase the photocathode surface. A miniature Hamamatsu PMT is also used for spectrometry purposes, as the channel PM tubes operate in saturated mode. The system is also equipped with a CdTe gamma detector and a ^{241}Am source, to allow its use as a Compton spectrometer [25]. Acquisition electronics is based on a locally developed FPGA module, including on-line coincidence and dead-time processing, and counters for coincident, non-coincident and time signals. The acquisition module is connected to a computer through a USB interface.

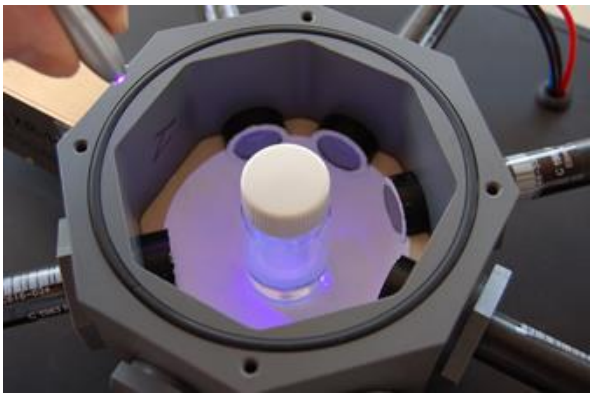

Figure 34. Internal view of the optical chamber of the CEA counter

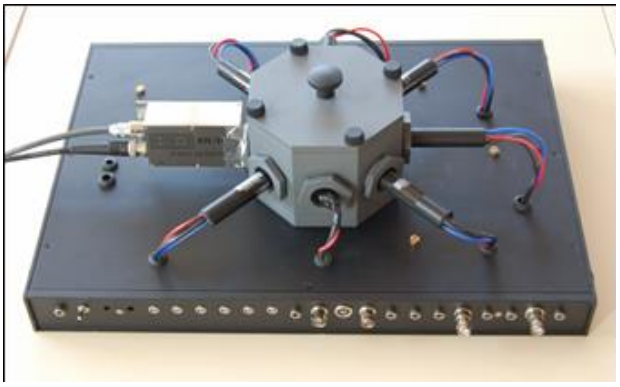

Figure 35. CEA TDCR counter

3.6.4 Validation

The validation of these prototypes has been completed in the developing laboratories by an inter-laboratory comparison of the activity measurement of a ^{3}H and a ^{241}Pu solution. It was observed that the detection efficiencies of portable counters of ENEA and NPL using dynode PM tubes are similar or slightly lower than

the ones of traditional TDCR counters used in these NMI. The counters of CEA and PTB using channel PMs exhibit a significantly lower detection efficiency than counters using dynode PM tubes. Nevertheless the first measurement results of low-energy emitters like ^{3}H are in very good agreement with the ones obtained using conventional TDCR counters, which is a good indicator of the quality of these portable instruments.

Conclusion

Portable TDCR counters were developed at ENEA, CEA, NPL and PTB, for the purpose of in-situ measurements of low-energy beta emitters at a nuclear site. These systems will also be useful in other contexts, like for the on-site measurement of short half-life radionuclides in production centers, or as a traveling metrological instrument for radionuclide activity inter-comparisons. First validation measurements of these instruments show that they are adequate for the purpose and yield activity values similar to the ones obtained with primary measurement systems in use in NMIs.

3.7 Digital Coincidence Counting

Many NMIs are particularly concerned by the problem of maintenance and renewal of their nuclear instrumentation and the current trend in the field is to make use of data acquisition systems based on high-speed digitisers, where the A/D conversion is performed as close as possible to the output of the detector or preamplifier (in contrast to traditional systems where A/D conversion usually appears at the end of the counting chain, following suitable analog processing of the detector signals).

These digital data streams, representative of the detector outputs, may be operated on by dedicated algorithms programmed onto Field Programmable Gate Arrays (FPGAs), such as digital filters, pulse shapers, constant fraction discriminators, timing filters, baseline restorers etc. Such algorithms are used to extract the quantities of interest from the large digitised data streams. In $4\pi\beta-\gamma$ coincidence counting, a method widely used by NMIs to provide primary standards of radioactivity, the quantities of most interest are the particle energy (proportional to the charge released by the particle in the detector) and the arrival time of the pulse.

These reduced data sets may be analysed to implement the $4\pi\beta-\gamma$ coincidence counting method by either processing the digital streams in “real-time” by using further dedicated algorithms programmed in FPGA-based devices, or to log the digitised pulse height and timing information in *list-mode* and process the information “off-line” via bespoke software routines.

Each of these approaches has its own merit, with the real-time approach offering a system capable of reporting the estimate of the source activity with little or no intervention from the operator. The list-mode approach offers an improved transparency in the calculations, where not only an estimate of the source activity can be reported, but the entire data set used in the determination estimate may be provided, for verification and validation. Other attractive advantages to the analysis of list-mode data sets is that the analysis algorithms may be readily programmed by a metrologist with no expertise in the programming of FPGAs, as well as the obvious freedom to “replay” the data sets through the software routines whilst altering a multitude of counting parameters (dead-times, gamma-gates, delays etc). In both cases, the real advantage of digitisation of the pulse trains is that the FPGA algorithms and/or the software analysis routines can be reprogrammed at any time, without the need to purchase additional hardware.

3.7.1 Front end electronics

The $4\pi\beta-\gamma$ coincidence method may employ a variety of detector types. For the detection of beta particles (as well as X-rays/Auger electrons following electron capture decay and internal conversion processes), proportional counters at both atmospheric and elevated pressures are commonly used, as are liquid scintillation detectors and plastic scintillators. For the detection of gamma photons, the use of NaI(Tl) and HPGe detectors are commonplace. Other detector configurations are obviously possible, and there are too many to list here in details. In some detector configurations, (i.e.: where a PMT is used) the signal strength is often sufficient to enable a direct coupling to the digitiser, without employing a preamplifier. However, careful consideration must be given to the input impedance of the A/D converters used, and it is often beneficial to employ additional dedicated front-end electronics to optimise the coupling to the A/D converter, in order to acquire an accurate representation of the electrical charge generated by the radiation detectors. For example, coupling the PMT from a high-efficiency NaI(Tl) detector to the CAEN digitiser (described later in this manuscript) yielded better results after employing the additional interface described in the next section. Such considerations are particularly important in order to achieve suitable low-energy thresholds to enable

extrapolation to zero energy where required and to minimise degradation of the signal to noise ratio. Due to space limitations, here we report our experiences on only a few of the possible detector configurations.

Digital Pulse Processing (DPP)

Two approaches were used to implement digital filters required to generate quantities of interest for a detected pulse: the particle energy (proportional to the charge released by the particle in the detector) and the arrival time of the pulse. The first approach was to construct our own implementations of appropriate digital filters, based on a recursive implementation of a Gaussian filter (and its derivatives). The second approach was to use a commercially available digitiser system with in-built Digital Signal Processing capabilities. Here we selected several modules from CAEN (DT5720, DT5724 and DT5751), (Figure 37), each operating with a different Digital Pulse Processing (DPP) firmware applied by the FPGA, with the relevant energy and time-stamp information written to file for subsequent software processing. The digital filtration operates to perform noise rejection, baseline cancellation and perform shape and timing analysis. The timestamp generation is performed by transforming the pulses into bipolar signals where zero crossing (pulse amplitude independent) can be used for accurate determination of the time stamp.

Figure 37. The CAEN DT5720 digitiser.

Implementation of a Recursive Gaussian Digital Filter

The recursive implementation of a Gaussian filter (and its derivatives) originally proposed by Young and van Vliet [30] for computer vision (image filtering, edge detection, etc.) was deemed a suitable candidate for construction of the digital filter. The algorithms were specifically developed for the processing of signals generated by photons detected in a high-efficiency well-type NaI(Tl) detector and a Silicon Drift Detector (SDD). In both cases, we used front-end electronics especially designed to optimise the coupling between the analog part and the digitisation stage (14 bits, 125 MHz, installed in the Stratix III development kit) as described above. These algorithms (developed in MATLAB®) were applied to digitised pulse trains according to an off-line processing in a development phase in order to be programmed in future FPGA circuitry for on-line processing for routine measurements.

The actual implementation of the Gaussian filter algorithm was reported elsewhere [31]. A smoothing filter (8-sample averaging) is first implemented on the digitised pulse trains in order to obtain a new original signal with an improved signal-to-noise ratio. The algorithm is then applied as a low-pass filter for pulse-height analysis corresponding to the “slow channel” in a classical instrumentation environment. The leading-edge detection is computed in the “fast channel” which uses the 1st derivative of the Gaussian filter. This differential operator generates fast signals that are used to trigger the dead-time management, the counting and the pulse-height analysis in the “slow channel”.

The Laplacian filter (2nd derivative of the Gaussian filter) is applied for pile-up identification by monitoring zero-crossings. (Figures 38 and 39).

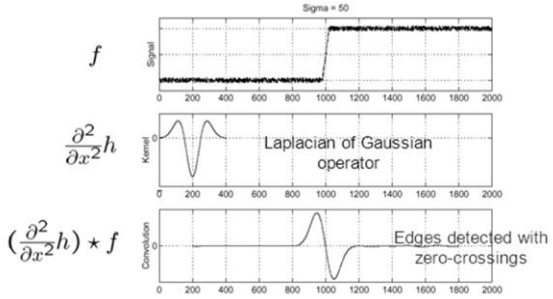

Figure 38. Recursive Gaussian DPP Filter used for edge detection and timing optimisation. The digitised input signal from the front end electronics, f, undergoes a convolution with the second derivative (or Laplacian operator) of the Gaussian filter.

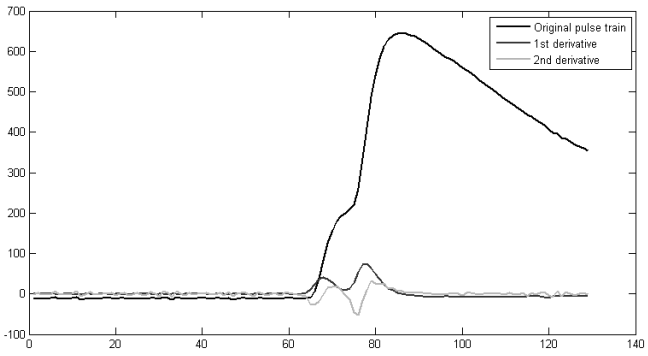

Figure 39 (x-axis scale: x 64 ns). Example of the use of the algorithm for pile-up identification based on zero-crossing detection using the 2nd derivative of the Gaussian filter. The separation between output pulses is ~ 600 ns, which is of the order of the rise time of the input pulse.

The detection of local maxima of the 1st derivative can be also used as a form of Constant Fraction Discriminator (CFD) to reduce the jitter-effect on the signal triggering. An example of the processing of the extendable dead time using the signals generated in the "fast channel" is given in Figure 40 (minimum duration set to 300 samples corresponding to ~ 19 μs).

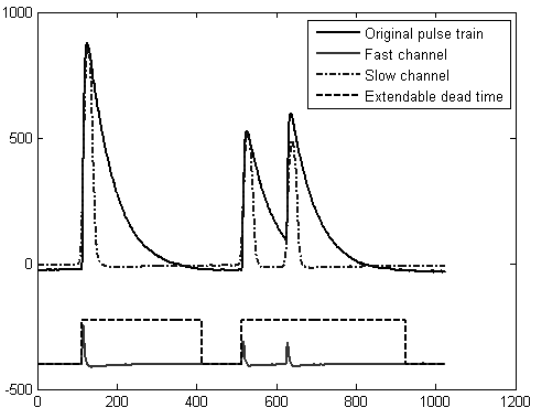

Figure 40 (x-axis scale: x 64 ns). Digital pulse processing applied to signals delivered by a high-efficiency well-type NaI(Tl) detector. The "fast channel" is used to trigger the extendable dead-time management (minimum duration equal to 300 samples) and the pulse-height analysis in the "slow channel".

Considering the "slow channel", the differentiation is first computed by subtracting from the original pulse train the attenuated and delayed (24 samples, ~ 1.5 μs) original signal. The pole-zero compensation is set by

the magnitude of the attenuation. The mean value of the offset on the original pulse train is continuously estimated prior the dead-time triggering. For the pulse-height analysis, the differentiated signal is smoothed using another implementation of the Gaussian filter. The amplitude is given by the first maximum value corrected for the baseline level of the differentiated signal measured prior the dead-time triggering.

CAEN DPP-CI (Charge Integration)

The CAEN Charge Integration DPP firmware (DPP-CI) was implemented in the Model DT5720 (12 bit, 250MS/s) as well as the Model DT5751 (10 bit, 1GS/s) which were used to directly digitise the outputs from PMTs connected to Liquid Scintillation Counters and NaI(Tl) detectors, where the output pulses are of sufficient magnitude without the need for extra front end electronics. The DPP-CI forms the equivalent of an analog chain comprising a Charge Integrating ADC (QDC), discriminator and gate generator, and operates as shown in Figure 41 and Figure 42.

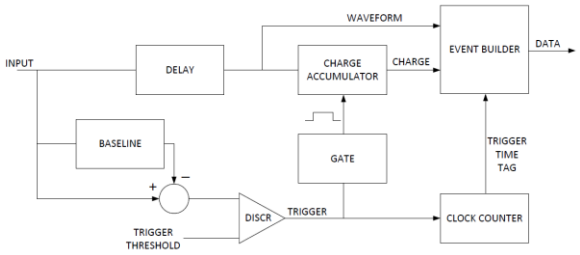

Figure 41. Schematic representation of the CAEN DPP-CI firmware implementing the charge integration algorithm.

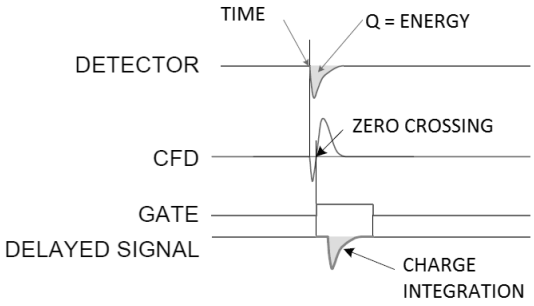

Figure 42. Digital signals created in the DPP-CI firmware.

The DPP-CI integrates the total input charge but requires a gate signal to define the integrating window. This is generated from the input signal itself and requires splitting of the digitised input signal so that it is passed to both the discriminator (CFD) algorithm and also delayed so that the start of the input signal is aligned with the gate trigger. The zero-crossing of the derivative of the input signal is used to start this gate period, the length of which is matched to the width of the input signals. Further details may be found in the manufacturers Application Note [32].

CAEN DPP-PHA (Pulse Height Analysis)

The CAEN Pulse Height Analysis firmware (DPP- PHA) was implemented in the Model DT5724 (14 bit, 100MS/s) which was used to digitise the outputs from several charge sensitive preamplifiers and detector systems, as described in Section II. The DPP-PHA implements a “trapezoidal filter” or “moving window deconvolution filter” [33] which transforms the exponential shape of the input signal to a trapezoidal pulse with height proportional to the input pulse magnitude, via recursive convolution algorithms. The exponentially decaying input signal from the charge sensitive preamplifier is first convolved with a rectangular function, followed by a truncated ramp function. (Figure 43). Control of the filter parameters is achieved via user interaction with the control software. The DPP-PHA also generates a time stamp for each event, via means of a form of constant fraction discriminator, as described in the previous section, and thus logs the time and energy parameters in list-mode.

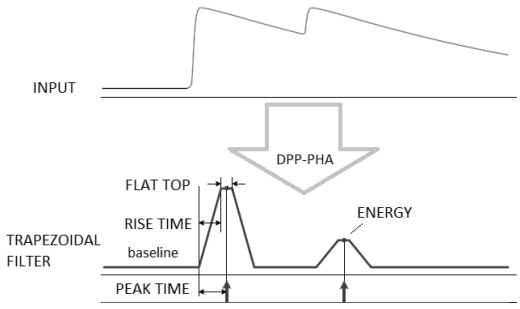

Figure 43. Operation of the digital trapezoidal filter used in the CAEN DPP-PHA firmware.

CAEN DPP-PSD (Pulse Shape Discrimination)

The CAEN Pulse Shape Discrimination DPP firmware (DPP-PSD) may be implemented in in the Model DT5720 (12 bit, 250MS/s) as well as the Model DT5751 (10 bit, 1GS/s). The algorithms used are similar to those used in the DPP-CI firmware, but in this instance two charge integration gates (of short and long duration) are used. Prior to registration of an event, the baseline of the input stream is calculated via a moving average filter. This baseline level is subtracted from the input signal, and if the resulting digital code exceeds the user specified threshold level, a trigger is issued, and the baseline held constant. The two gates of user defined width are used to perform the charge integration, after applying a suitable delay to a copy of the input signal to ensure optimal charge integration. The time stamp of the trigger is calculated as described in the previous sections and logged to a list-mode data file along with the charged collected within the two gates. On completion of the "long" gate, the moving average baseline filter is restarted, and the process repeats with each subsequent pulse arrival. The DPP-PSD firmware then logs the time stamp, and the charge from both gates in list-mode. Although this DPP is designed for neutron-gamma discrimination in liquid scintillation detectors, one can easily operate this in the same manner as the DPP-CI by only utilising the charge data from the "long" gate. Preliminary tests have been performed at ENEA-INMRI with the CAEN DT5720B device directly coupled to a homemade portable TDCR counter [34], [35], developed in the project, by using a source of mixed ^{241}Am and ^{90}Sr for α/β separation with the PSD technique.[34], [36].

3.7.2 Coincidence Counting on list-mode data files

Standard DCC data format

The list-mode data format from each of the above digitiser systems is unique, and in order to implement the $4\pi\beta-\gamma$ digital coincidence counting (DCC) technique, a standard binary data format to pass between software functions was required. At present, there is no international standard data format for such measurements, and thus there are no "off the shelf" software routines to mimic the operation of the analogue electronic modules required to implement $4\pi\beta-\gamma$ digital coincidence counting. A standard binary data format was developed within the project consortium, and all analysis routines used were produced as part of this project to accept data in this format. In all cases, the first function to be called is a data conversion routine, altering the various list-mode ASCII and binary data formats to this standard format.

Furthermore, a major outcome from this project was the development of an internationally recognised standard data format. To this end, the DCC leader from the project now leads a task within the newly established ERNCIP (European Reference Network for Critical Infrastructure Protection) Thematic Group on the Protection of Critical Infrastructure from Radiological and Nuclear Threats, which is pursuing the development of such a standard for list-mode data sets in radionuclide metrology. Proposals are presently being drafted to both the European Committee for Electrotechnical Standardisation (CENELEC) and the International Electrotechnical Commission (IEC) Technical Committee 45 on nuclear instrumentation.

Support for this project has also been received from the International Committee for Radionuclide Metrology (ICRM) Working Group on Radionuclide Metrology Techniques.

DCC analysis software

Data files (after conversion to the project's internal data format) are then passed to a suite of dedicated software routines for an off-line implementation of the $4\pi\beta-\gamma$ digital coincidence counting (DCC) technique. These routines include: dead time imposition, pulse interval digitisers, single channel analysers, logic width and delay imposition, coincidence mixers, scalers, live-timers, multichannel analysers etc.).

In all stages of software development a highly modular design was used to readily facilitate the testing and validation of the various software components. The DCC data analysis routines were compiled in C++ as exportable functions residing in a 32-bit Dynamic Link Library (DLL), and the graphical user interface used to call these routines and present data to the user for interaction were compiled under the LabVIEW environment. A primary radionuclide standardisation by the $4\pi\beta-\gamma$ coincidence counting technique typically requires the processing of several millions of pulses (in order to achieve the required statistical precision) and since the user of the DCC system is free to replay the collected data sets through a range of different counting regimes, a great deal of emphasis was placed on maximising the software execution speed.

DCC data simulation
The validation of the correct operation of the DCC routines formed a major part of the project, and proceeded via the development (again in C++) of a Monte Carlo simulation program which generates digital data-sets with known characteristics for a simple simulated beta – gamma emitting nuclide in the appropriate format.

Inputs to the Monte Carlo model include: the total number of disintegrations to simulate, the source activity, the ADC sampling frequency, the detector efficiencies for various nuclear and atomic emanations, the beta channel spectral shape, the internal conversion coefficient for the gamma transitions, simulated pulse widths and random jitter, among many others. Appropriate transformations of uniform random variations are used to determine the exponentially distributed intervals between successive nuclear disintegrations, the amplitudes assigned to registered pulses and their final time stamps.

For each simulated nuclear disintegration, a beta particle was yielded with a pulse height sampled from the input beta spectral shape distribution. According to the input internal conversion coefficients, either a simulated gamma ray or conversion electron is produced. The fate of these particles is determined according to the input detector efficiency parameters.

The fact that the simulated pulses exhibit finite widths and exponentially distributed inter-arrival times leads to the possibility of pulse pile-up occurring between responses due to different parent decays. The model keeps a record of all recorded pulse start-times and pulse-shapes from each channel, performs a summation of the responses where appropriate and “extends” the pulses accordingly. The time assigned to each event registered is constructed from the sum of all prior intervals, augmented with any simulated random time “jitter” and/or constant delay.

Extensive testing of the operation of the DCC analysis routines with these simulated data sets proved invaluable in the development (and associated debugging) of the software. In all cases, the output of the routines agreed with simulation inputs, demonstrating correct behavior.

Conclusion

Significant progress was made towards the enhancement of portable, robust (and transparent) primary standards of radioactivity. Signals from various radiation detectors have been digitally sampled at state-of-the-art sampling frequencies (10^8 - 10^9 samples per second). The software for analysing these recorded pulse trains is complete and will routinely be used in international comparison exercises for reporting the activity concentration for a variety of nuclides. An international effort is underway to develop a standard data format for “list-mode” data sets used in radionuclide metrology.

4 Actual and potential impact

Main Dissemination Activities and exploitation of Results

In terms of dissemination of the project results, the project coordinator was invited as a keynote speaker at the IMEKO2011 conference in Dubrovnik in June 2011 and at the ANIMMA conference in Marseille June 2013. The project also had a special session at the same conference and seven papers have been accepted for publication. Contributions have been made to the SNETP (Strategic Nuclear Energy Technology Platform) Newsletter and several trade magasines (e.g. Materials Worls and Nuclear Future). This SNETP is a very important European platform for political decisions regarding future nuclear power in Europe and the project was presented at the SNETP General Assembly in November 2011. In total, more than 36 peer-reviewed papers describing the scientific achievements of the project have been submitted to peer-reviewed journals and more than sixty presentations has been given at conferences and workshops such as

Metrologie, ITS, ICRM, Tempmeko and ANIMMA. The work was presented at an SP/EDF Workshop in Paris. During these conference contacts were made with major stakeholders e.g. IRSN, CEA-DEN and AREVA.

The project held an open meeting to users and stakeholders, in Rome, 9-10 February 2012. Representatives from the SNETP, the ITER Fusion project and Digital Electronics providers attended the meeting. In October 2012, project partners went to the Generation IV project ASTRID in Cadarache, France, to disseminate the results of the project to CEA, France (which are building the test reactor Jules Horowitz in Cadarache). Finally, in June 2013, the project held a workshop dedicated to Nuclear Data, the INDD 2013, where stakeholders were presented with the improved nuclear data from this project. The workshop was organised by IFIN-HH and SMU together with the JRC.

Furthermore, national representatives have been identified for the three major standard committees related to the scientific developments in this project; ISO, IEC and IAEA and input has been provided, with a technical note that presents project results and suggested changes to current standards.

Scientific Impact

New high temperature reference/s tailored to assess performance of current and new thermocouples

The collaborative work in this project supported the realisation of new references and sensors which can be made readily usable in the field of nuclear energy and will be usable in the next generation of nuclear power plants:

- A new temperature reference point at the Fe-C eutectic was developed and characterised. Its melting temperature in the international temperature scale was assigned by NPL, LNE and CNAM. This point can be applied for thermocouple drift studies. It can also be used for calibration services.
- A practical acoustic thermometer was developed and tested successfully up to temperatures as high as 1000 °C. This kind of thermometer, once miniaturised, would be very useful for temperature measurements in harsh environments.
- Self-validation techniques have been developed and tested at the Fe-C point in particular and show their suitability for in-situ drift correction of thermocouples.

Improved thermochemical data and modelling for nuclear design

New critically assessed thermodynamic data have been derived to model the interaction between a liquid sodium coolant and the nuclear fuel, containment materials and fission products. This will enable better predictions to be made of potential nuclear accident scenarios necessary for the development of a liquid sodium generation IV nuclear reactors.

Thermophysical properties of advanced materials

The collaboration between LNE, PTB, NPL and JRC has enabled the implementation of metrological facilities in order to provide reliable and traceable high temperature measurements for materials having thermal properties similar to those used in fission reactors. The main scientific impact is:

- Extension of the temperature range (up to 2000 °C) for which traceable thermal diffusivity measurements can be performed on homogeneous solid materials,
- Possibility to obtain traceable normal spectral emissivity measurements of solid materials up to 1500 °C,
- Availability of improved methods and calorimeters for the measurement of specific heat up to 1500 °C,
- Application of the developed apparatuses to the thermal characterisation of potential “transfer reference materials” for high temperature thermal properties measurements.

Nuclear data and nuclear instrumentation

The project outcomes/impact includes:

- Improvement of the alpha particle emission probabilities of ^{238}U by one order of magnitude.

- Implementation of a magnet system to avoid coincidence effects between alpha-particles and conversion electrons.
- Update of decay data library expected, that will have impact on alpha spectrometry in routine laboratories.
- Experience gained on effects of source preparation on the quality of alpha and beta spectrometry.
- Spectral shape of beta particle emission from ^{63}Ni and ^{241}Pu.
- Best experimental proof of existence of exchange effect in beta decay.
- More confidence in modelling of beta spectra.
- Capability to measure low-energy beta emitters in-situ
- Improved digital electronics and proposal of a new standards for digital data format

Socio-Economic / Policy Impact

At the end of the project there were many examples of the outputs being taken on by the relevant communities:

- Stakeholders such as the CEA-Cadarache, University of Marseille and IRSN were interested in collaborating and taking the developed temperature measurement capabilities one step closer to implementation in nuclear power plants and testing in reactors.
- Discussions have taken place with Elsevier to include the data produced by thermo chemical modelling within a revised version of “Thermochemical data for reactor materials and fission products”, last published in 1990. This is the key reference data source and will therefore make the new data developed by the project directly available to users the nuclear industry.
- The IAEA and the NEA/OECD have provided continued support for the development of neutron cross sections, of which the transfer instrument for neutron fluence measurements is an essential part.
- The nuclear decay data have been made available for evaluation by the Decay Data Evaluation Project (DDEP), the IAEA and the OECD/NEA nuclear data working groups.
- A digital electronics manufacturer has showed interest in further development and collaboration regarding the coincidence counting system (TCDR) developed in MetroFission as well as a continued collaboration with the European Networks (European Reference Network for Critical Infrastructure Protection).
- The digital electronics development also had a direct impact on the development of a new standard for nuclear instrumentation. One of the project partners has been asked to lead a task within the newly established ERNCIP (European Reference Network for Critical Infrastructure Protection) Thematic Group on the Protection of Critical Infrastructure from Radiological and Nuclear Threats, which is pursuing the development of such a standard for list-mode data sets in radionuclide metrology. Further proposals are presently being drafted to both CENELEC and IEC Technical Committee 45 on nuclear instrumentation. Support has also been received from the International Committee for Radionuclide Metrology (ICRM) Working Group on Radionuclide Metrology Techniques.
- The portable TDCR system has been taken up in another project, working on the development of a mobile laboratory for measurements of radioactivity at Sellafield Ltd. (UK).

The uptake of project outputs will lead to environmental, social and financial impacts. The environmental impact of this project comes from nuclear data and thermo-chemical modelling of proposed reactor fuels, as this will entail a closed fuel cycle, minimising waste and maximising efficient use of the fuel. The project will enable improved monitoring of radioactivity released into the environment during operation and waste management by improved measurements of radionuclides. Furthermore, the project has provided thermo-chemical and thermo-physical data for the safe design of new generation reactors as well as improved and new direct methods for temperature measurements.

The social impact of the project comes from improved metrology for safe construction and operation of the new generation reactors, that will contribute to an enhanced quality of life for European citizens. The financial benefits from the project will be from the development of better temperature measurement in

reactors which allows the production and use of high temperature reactors, capable of heat supply to improve efficiency and economy in a variety of industrial processes. The project has produced better and more reliable temperature measurements and sensors in reactors that will enable more efficient process control, reduced calibration and maintenance costs of temperature sensors and reduced costs for downtime. Previous experience of working with nuclear power plants has shown that there is a demand for on-site measurements as this significantly improves the efficiency and reduces the costs of the plant operation.

New high temperature reference/s tailored to assess performance of current and new thermocouples

A better knowledge of the temperature will always be of benefit for energy consumption and therefore for reduced socio-economic negative impact in general. The sensors and methods developed in this project will help increasing the reliability of the sensors and their traceability to the temperature standards.

Improved thermochemical data and modelling for nuclear design

In this project, data to model the interaction between a liquid sodium coolant and the nuclear fuel, containment materials and fission products have been developed which will provide basic information necessary for the development of a liquid sodium generation IV nuclear reactors.

Thermophysical properties of advanced materials

As part of the process of developing new fission reactors, a fundamental understanding of the thermal behaviour of the used materials at high temperature (structural and refractory materials, as well as irradiated and nuclear fuels) must be established, in particular to define the critical performance limitations of these materials and possible design alternatives. It is thus necessary to accurately determine the thermal properties of the materials concerned under temperature conditions close to those of in-pile operation and accident conditions (up to several thousand °C).

Thanks to the scientific outcomes of this project, the availability of accurate metrological facilities at the European level enables to improve the traceability to the SI of the measurements of thermal diffusivity, normal spectral emissivity and specific heat performed by the nuclear research laboratories up to 2000 °C, particularly for materials used in the design of generation IV reactors. A better understanding of the thermal behaviour of the materials will also enable an increase in the safety of the next generation of nuclear power plants.

Improved decay data

Improvement of decay data supports better modelling and calibration of measurement techniques, which enhances confidence in nuclear measurements and ultimately supports better informed science-based decision making.

Nuclear instrumentation

A major output from this project was to instigate the development of an internationally recognised standard data format. The partner leading the Digital Instrument development in this project now leads a task within the newly established ERNCIP (European Reference Network for Critical Infrastructure Protection) Thematic Group on the Protection of Critical Infrastructure from Radiological and Nuclear Threats, which is pursuing the development of such a standard for list-mode data sets in radionuclide metrology. Proposals were drafted to both the European Committee for Electrotechnical Standardisation (CENELEC) and the International Electrotechnical Commission (IEC) Technical Committee 45 on nuclear instrumentation using the projects outputs. The latter accepted this proposal and a draft new version of a standard is being written by a working group within TC45. Support for this proposal has also been received from the International Committee for Radionuclide Metrology (ICRM) Working Group on Radionuclide Metrology Techniques.

5 Website address and contact details

http://projects.npl.co.uk/metrofission/

Contact details:

Lena Johansson	NPL	+44 20 8943 8587	lena.johansson@npl.co.uk
Bruno Chauvenet	CEA	+33 1 69 08 89 81	bruno.chauvenet@cea.fr
Dolores del Campo	CEM	+34 918 074 714	ddelcampo@cem.mityc.es
Miguel Embid	CIEMAT	+34 913 466 079	m.embid@ciemat.es
Jana Sochorova	CMI	+42 026 602 04 22	jsochorova@cmi.cz
Mohamed Sadli	CNAM	+33 1 40 27 20 23	mohamed.sadli@cnam.fr
PierinoDe Felice	ENEA	+39 06 304 835 80	pierino.defelice@enea.it
Aurelian Luca	IFIN-HH	+40 21 404 61 63	aluca@ifin.nipne.ro
Arjan Plompen	JRC(IRMM)	+32 145 713 81	arjan.plompen@ec.europa.eu
Konstantinos Boboridis	JRC(ITU)	+49 7247 951305	konstantinos.boboridis@ec.europa.eu
Jean-Remy Filtz	LNE	+33 1 30 69 12 15	jean-remy.filtz@lne.fr
Dirk Arnold	PTB	+49 531 592 6100	dirk.arnold@ptb.de
Jaroslav Compel	SMU	+421 2 602 94 665	compel@smu.gov.sk

6 References

[1] Johansson, L., Filtz, J. R., De Felice, P., Sadli, M., Plomben, A., Hay, B., Dinsdale, A., Pommé, S., Cassette, P., and Keightley, J., "Advanced Metrology for New Generation Nuclear Power Plants", in proceedings of 2nd IMEKO TC11 International Symp. Metrological Infrastructure: Cavtat, Croatia, 2011, pp. 15-17.

[2] Sadli M., del Campo D., de Podesta M., Failleau G., Fourrez S., Garcia C., Pearce J., Rae C., Scervini M., "Improving high temperature measurements for the nuclear industry at the European level", in electronic proceedings of 15th Int. Congress of Metrology, 2011.

[3] Elliott, C. J., Pearce, J. V., Failleau, G., Deuzé, T., Briaudeau, S., Sadli, M., and Machin, G., "Fe-C eutectic fixed-point cells for contact thermometry: an investigation and comparison", Metrologia 49, 88-94 (2012).

[4] Failleau, G., Deuzé, T., Pearce, J. V., Elliott, C. J., Machin, G., Briaudeau, S., and Sadli, M., "Development of an Fe-C Eutectic Fixed-Point for the Calibration and In-Situ Monitoring of Thermocouples", in Proceedings of 2nd IMEKO TC 11 International Symposium Metrological Infrastructure: Cavtat, Croatia, 2011, pp. 77-80.

[5] Sadli M., del Campo D., de Podesta M., Failleau G., Elliott C.J., Fourrez S., Garcia C., Pearce J.V., "MetroFission: New High-Temperature References and Sensors for the Nuclear Industry", *Temperature: Its Measurement and Control in Science and Industry*: Vol 8: (2013).

[6] de Podesta, M., Sutton, G., Underwood, R., Legg, S., Steinitz, A., Int J Thermophysics (2010) 31:1554-1566.

[7] Sutton G. , de Podesta M., Veltcheva R, Gélat P., Minh H.D., and Edwards G. *Temperature: Its Measurement and Control in Science and Industry*: Vol 8: (2013).

[8] Yamada Y., Sakate H., Sakuma F., Ono A., "High-temperature fixed points in the range 1150 °C to 2500 °C using metal-carbon eutectics" Metrologia, 38, p 213-219 (2001).

[9] Sadli M., Bourson F., Fanjeaux M., Briaudeau S., Rougié B., Bonnier G. "Study Of Metal-Carbon Eutectic Points : From Construction To Temperature Determination" in Proc. 9th Int. Symp. on Temperature and Thermal Measurements in Industry and Science (Tempmeko) (Dubrovnik) pp 611-6 (2004).

[10] Ongrai O., Pearce J. V., Machin G. and Sweeney S. J. "Miniature Co–C eutectic fixed-point cells for self-validating thermocouples", Meas. Sci. Technol., 22 015104 (2011).

[11] O. Ongrai, J.V. Pearce, G. Machin and S.J. Sweeney "A miniature high temperature fixed point for self-validation of Type C thermocouples", Meas. Sci. Technol., 11 105103 (2011)

[12] Rempe, J. L., and Wilkins, S. C., "High Temperature Thermocouples for In-Pile Applications", in Proceedings of The 11th International Topical Meeting on Nuclear Reactor Thermal-Hydraulics (NURETH-11): Avignon, France, 2005, pp. 2-6.

[13] Knudson D.L., Rempe J. L., Condie K. G., Wilkins S. C., Daw J. E. and Crepeau J. C. "High Temperature Irradiation Resistant Thermocouples – A Low Cost Sensor for In-Pile Testing at High Temperatures" in Proceedings of ICAPP '08, Anaheim, CA USA, June 8-12, 2008.

[14] Villard, J. -F., Fourrez, S., Fourmentel, D., and Legrand, A., “Improving High-Temperature Measurements in Nuclear Reactors with Mo/Nb Thermocouples” Int. Journal of Thermophysics 29, 1848-1857 (2008).

[15] Fourrez S., Villard J. F., Laurie M., “Perspective de mesures à haute température sous irradiation à l’aide de thermocouples type N et Mo/Nb” presented at Journée SFT “Mesures intrusives des hautes temperatures” 29 june 2010, Cnam, Saint-Denis, France (2010).

[16] Pitre L., Sparasci F., Truong D., Guillou A., Risegari L. and Himbert M. E., Measurement of the Boltzmann Constant kB Using a Quasi-Spherical Acoustic Resonator. Int. J. Thermophys (2011) 32, 9, 1825-1886.

[17] Yazaki, T., Tashiro, Y., Biwa, T., Proc. R. Soc. A (2007) 463, 2855-2862, doi:10.1098/rspa.2007.1897.

[18] Brochure for Fe-C fixed point realisation at NPL and LNE and CNAM : http://lcm.cnam.fr/Metrofission/brochurefec.pdf

[19] Report of the SNETP Fukushima task group “Identification of Research Areas in Response to the Fukushima Accident”, January 2013 http://www.snetp.eu/www/snetp/images/Fukushima_report_HD.pdf.

[20] M. Capogni, P. De Felice, S. Loreti. Metrofission Project: an overview of the ENEA contribution. Submitted to the International Workshop energy 2012-CMAM Madrid, Spain.

[21] M. Capogni, P. De Felice. A prototype of portable TDCR system at ENEA. Submitted to the LSC 2013 conference.

[22] Bouchard, J. and Cassette, P.. MAC3: an electronic module for the processing of pulses delivered by a three photomultiplier liquid scintillation counting system .Applied Radiation and Isotopes, Volume 52, Issue 3, March 2000, pp 669-672.

[23] L. Johansson, E. Bakhshandeiar, A. Pearce, P. Orlandini, J. Sephton. A miniature TDCR system dedicated to in-situ activity assay. Submitted to the ICRM 2013 conference.

[24] O. Nähle, Q. Zhao, C. Wanke, M. Weierganz, K. Kossert. A portable TDCR system. Submitted to the ICRM 2013 conference.

[25] P. Cassette and P. Do. The Compton Source Efficiency Tracing method in Liquid Scintillation Counting, a new standardization method using a TDCR counter with a Compton spectrometer. Applied radiation and Isotopes Vol 66, Issue 6-7 (2008), pp 1026-1032.

[26] http://root.cern.ch/drupal/

[27] P. Butkus, M. Capogni, A. Gudelis. Development of a new software for the off-line TDCR coincidence counting analysis. Poster S3-64, 40th Lithuanian National Physics Conference (LNFK-40), 10-12 June, 2013, Vilnius, Lithuania.

[28] K. Kossert, P. Cassette, A. Grau Carles, G. Jörg, Ch. Lierse v. Gostomski, O. J. Nähle, Ch. Wolf. Extension of the TDCR model to compute counting efficiency for radionuclides with complex decay scheme. Submitted to the ICRM 2013 conference.

[29] C. Bobin, J. Bouchard, S. Pierre and C. Thiam, “Overview of a FPGA-based nuclear instrumentation dedicated to primary activity measurements”, *Appl. Radiat. Isot.*, vol. 70, pp. 2012-1017, 2012.

[30] I.T. Young and L.J. van Vliet, “Recursive implementation the Gaussian filter”, *Signal Process*. vol. 44, pp. 139–151, 1995.

[31] C. Bobin. “Digital pulse processing and optimization of the front end electronics for nuclear instrumentation”, to be published.

[32] *Charge Integration: Analog Vs. Digital, CAEN Application Note AN2503*, CAEN SpA, Viareggio, Italy, 2010.

[33] V.T. Jordanov and G.F. Knoll, “Digital Synthesis of pulse shapes in real time for high resolution radiation spectroscopy”, *Nucl. Inst. Meth. A*, vol. 345, pp. 337-345, 1994

[34] M. Capogni, P. De Felice. « A prototype of a portable TDCR system at ENEA”. To be published, LSC 2013 conference.

[35] P. Cassette, M. Capogni, P. De Felice, L. Johansson, K. Kossert, O. Nahle, J. Sephton. “Development of portable Liquid Scintillation counters for on-site primary measurement of radionuclide using the Triple to Double Coincidence Ratio method”. Submitted to ANIMMA conference, June 2013

[36] P. Butkus. “Study of the TDCR technique by a newly developed software for the off-line coincidence counting and digitized data analysis”. Thesis carried out at ENEA-INMRI (Supervisor: M. Capogni) in the frame of the ERASMUS EU Lifelong Learning Programme for the degree of Bachelor in Physics of Nuclear Energy. Faculty of Physics, Vilnius University. Lithuania. June 2013